Non-Statistical Effects in the Fragmentation of Electronic States of Gas-Phase Polyatomic Molecular Ions

Hatherly, P. A.; Smith, D. M.; Tuckett, R. P.

DOI:
10.1524/zpch.1996.195.Part_1_2.097

Zeitschrift für Physikalische Chemie, Bd. 195, S. 97–136 (1996)

Non-Statistical Effects in the Fragmentation of Electronic States of Gas-Phase Polyatomic Molecular Ions

By P. A. Hatherly[1], D. M. Smith[2]* and R. P. Tuckett[2]

[1] Department of Physics, University of Reading, Whiteknights, Reading RG6 2AK, UK
[2] School of Chemistry, University of Birmingham, Edgbaston, Birmingham B15 2TT, UK

Dedicated to Prof. Dr. H. Baumgärtel on the occasion of his 60th birthday

(Received November 25, 1995; accepted March 4, 1996)

Synchrotron / Coincidences / Threshold electrons / Non-statistical processes / Polyatomic cations / TPEPICO, PIFCO and TPEFCO

Using coincidence techniques and vacuum-UV radiation from a synchrotron source, the decay channels of the valence electronic states of a range of 4–7 atom polyatomic molecular cations in the gas phase have been determined. In particular, threshold photoelectron – photoion coincidence (TPEPICO), photoion–fluorescence coincidence (PIFCO), and threshold photoelectron–fluorescence coincidence (TPEFCO) spectroscopies have been used to measure, state selectively, the decay pathways in excited states of CF_4^+, CF_3Cl^+ and CF_3Br^+, $SiCl_4^+$ and BCl_3^+. Electrons, ions and photons are detected by threshold electron analysis, time-of-flight mass spectrometry and undispersed fluorescence, respectively. TPEPICO spectra are recorded both continuously as a function of photon energy, allowing threshold photoelectron spectra and yields of the fragment ions to be determined, and at a fixed photon energy with good time resolution, allowing mean translational kinetic energy releases, $\langle KE \rangle_t$, to be measured. By comparing $\langle KE \rangle_t$ values with those predicted for the limiting extremes of a statistical and an impulsive dissociation process, information on the nature of the photodissociation dynamics can be inferred. PIFCO and TPEFCO spectra are only recorded at fixed photon energies. The former experiment can yield the fate of the lower electronic state of the parent ion to which fluorescence occurs, the latter the lifetime of the fluorescing state; with sufficient resolution in the photon beam, the lifetime is specific to one vibrational level of the emitting state. Radiative decay and large $\langle KE \rangle_t$ values are two manifestations of isolated-state, non-statistical behaviour. None of the ions studied are large enough to be in the 'large-molecule' limit, and many non-statistical effects are observed in the decay of their excited states.

* *Present address:* Department of Chemistry, University of Southampton, Highfield, Southampton SO17 1BJ, UK.

Mittels Koinzidenztechniken und Vakuum-UV-Bestrahlung mit einer Synchrotronquelle wurden die Zerfallswege einer Reihe von 4–7 atomigen Molekülkationen in der Gasphase, nach Anregung ihrer Valenzelektronen in angeregte Zustände, bestimmt. Threshold photoelectron-photoion coincidence (TPEPICO), photoion–fluorescence coincidence (PIFCO), und threshold photoelectron–fluorescence coincidence (TPEFCO) Spektroskopie wurden verwandt, um die Zerfallswege von CF_4^+, CF_3Cl^+ and CF_3Br^+, $SiCl_4^+$ und BCl_3^+, in Abhängigkeit der elektronisch angeregten Zustände zu vermessen. Elektronen, Ionen und Photonen wurden jeweils durch Schwellenwert-Elektronenanalyse, zeitaufgelöste Massenspektroskopie und nicht-disperse Fluoreszenz detektiert. TPEPICO-Spektren wurden sowohl kontinuierlich in Abhängigkeit von der Photonenenergie aufgezeichnet, um Schwellenwert-Photoelektronen-Spektren und die Ausbeute der Fragmentionen zu erhalten, als auch bei festgelegten Photonenenergien mit hoher Zeitauflösung durchgeführt, um die mittleren kinetischen Translationenergie-Abnahmen $\langle KE \rangle_t$ zu ermitteln. Durch Vergleich der $\langle KE \rangle_t$-Werte mit den berechneten $\langle KE \rangle_t$-Werten für statistische oder impulsinduzierte Dissoziationsprozesse konnte Einblick in die Natur der Photodissoziations-Dynamik gewonnen werden. PIFCO- und TPEFCO-Spektren wurden nur bei bestimmten Photonenenergien aufgenommen. Durch PIFCO-Spektroscopie wurde das Verhalten der niedrigeren elektronisch angeregten und fluoreszierenden Zustände der Ionen untersucht. Mittels TPEFCO-Spektroskopie konnte die Lebensdauer des Fluoreszenz-Zustandes erfaßt werden. Bei ausreichender Auflösung des Photonenstrahls war diese Lebensdauer spezifisch für ein Schwingungs-Niveau des Emmissions-Zustandes. Die Strahlungsabnahme zusammen mit großen $\langle KE \rangle_t$-Werten in Verbindung mit weiteren Ergebnissen wiesen auf ein zustands-isoliertes, nicht-statistisches Verhalten hin. Dies ließ darauf schließen, daß die untersuchten 4–7 atomigen Molekülkationen nicht zu Großmolekülen gerechnet werden können.

1. Introduction

This short review will describe some families of gas-phase polyatomic molecular ions whose excited states show interesting and unexpected decay properties. The compounds of interest are the halogenated ions of groups III and IV of the periodic table, and we are now starting to extend these studies to the group V cations. These cations have valence states which lie ca. 10–25 eV above the ground state of the neutral molecule, and this paper describes experiments using tunable vacuum ultra-violet (VUV) radiation from a synchrotron as a photoionisation source to measure the different decay properties of these states.

Molecular ions are transient, free radicals whose importance in comets, the interstellar medium, and flame chemistry (to name but three examples) is now widely appreciated. The last twenty years have seen an enormous growth in techniques to study both their spectroscopic and dynamic properties. In any spectroscopic experiment the primary aim must be to produce as high a concentration of the molecular ion of interest as possible, and the presence of unwanted species is not important so long as they do not mask the spectral features of the ion. This explains why the relatively simple and cheap method of electron impact and many different forms of electrical discharge have been popular methods for producing ions for spectral charac-

terisation [e.g. 1, 2]. A dynamics experiment has different requirements. To study the decay of an isolated state of a gas-phase ion, the aim now must be to produce only that state of the ion, and ideally with a known concentration. Non-resonant excitation methods such as electron impact or electrical discharge are no longer suitable, and techniques using photons are usually employed.

Consider photoionisation of a general, halogenated polyatomic molecule MX_n (where M = B, C, Si, Ge; X = F, Cl, Br; n = 3,4)

$$MX_n + h\nu \rightarrow MX_n^{+(*)} + e^- \tag{1}$$

MX_n^+ may form in the ground or an excited state (labelled*). This process is described as non-resonant because if the photon energy exceeds that needed to produce $MX_n^{+(*)}$, the electron can carry away the energy difference between that of the photon and that of $MX_n^{+(*)}$ as excess kinetic energy (KE). If the KE of the electron is defined by some sort of energy analyser, then $MX_n^{+(*)}$ is 'state-selected', and with sufficient resolution in both the incident photon beam and the electron energy analyser vibrational state-selectivity in $MX_n^{+(*)}$ can often be achieved. In this work we use a threshold electron analyser to detect only those electrons which have essentially zero kinetic energy. The state-selected $MX_n^{+(*)}$ then corresponds to that state of the ion produced in the Franck-Condon region at an energy defined by the photon energy $h\nu$. This is the usual way to select a vibronic state of the molecular ion if a tunable photon source such as a synchrotron is available. We use a range of coincidence techniques to measure the decay properties of such isolated states of polyatomic ions. These include the threshold photoelectron–photoion coincidence (TPEPICO), the photoion–fluorescence coincidence (PIFCO) and the threshold photoelectron–fluorescence coincidence (TPEFCO) techniques. Full details are given in Section 3.

It is generally accepted that there are two limiting extremes to the form of the dissociation dynamics of excited states of molecular ions (and, indeed, neutral molecules). These are called the 'dynamical' and the 'statistical' limits, and apply to small and large molecular ions respectively. If we consider the possible decay routes of an electronically excited state of MX_n^+, it can decay both by radiative and non-radiative routes:

$$MX_n^{+*} \xrightarrow{k_{rad}} MX_n^{+(*)} + h\nu$$

or

$$MX_n^{+*} \xrightarrow{k_{non\text{-}rad}} \text{fragment ions} + \text{neutral(s), e.g. } MX_{n-1}^+ + X \tag{2}$$

k_{rad} and $k_{non\text{-}rad}$ are unimolecular rate constants for radiative and non-radiative decay respectively, and fluorescence may occur to the ground state or to a lower-lying excited state of the ion. Diatomic and most triatomic ions exhibit the properties of dynamical behaviour, of which four are pertinent

to this paper. First, potential energy curves and spectroscopic term symbols are useful descriptions of the excited electronic states of the ion. Second, fluorescence from excited states is as common a phenomenon as direct dissociation or predissociation, i.e. k_{rad} may be greater than, comparable to, or less than $k_{non\text{-}rad}$. Whether a state fluoresces or exhibits non-radiative decay depends on the detailed topography of the excited state of interest and how this state interacts with nearby electronic states. Third, fragment or daughter ions have appearance energies which relate to the particular electronic state of the parent ion which dissociates to that daughter ion. Thus appearance energies are often substantially higher in energy than the thermochemical threshold for production of that ion. Fourth, for photon energies in excess of a particular appearance energy the fraction of the available energy released into translational kinetic energy of the products is usually large; in the limit of a diatomic ion dissociating to an atomic ion + atomic neutral (e.g. $O_2^+ \rightarrow O^+ + O$), then of course this fraction is unity.

Large molecular ions exhibit very different properties of statistical behaviour. First, potential energy curves and the spectroscopic labelling of individual states generally are not important guides to the behaviour of an excited electronic state of the parent ion because it is assumed that non-radiative processes, especially internal conversion, occur so rapidly between electronic states that only the dissociation dynamics of the *ground* state have to be considered. Second, it follows that fluorescence from excited states is a very minor channel, especially if the state of interest lies above the energy of one or more fragmentation channel, i.e. $k_{rad} \ll k_{non\text{-}rad}$. Third, the fragmentation dynamics are governed by dissociation from the ground-state potential energy surface. Unless there is a substantial barrier in the exit channel to dissociation, daughter ions have an appearance energy which is very close to that of the thermochemical threshold for production of that ion. Fourth, for photon energies above this limit the fraction of the available energy that is released as translational KE of the products is usually small. Furthermore, the larger the ion the smaller this fraction is, because of the larger density of internal (rotational and vibrational) energy states of the daughter ion.

Dissociation rates from the ground-state potential can be quantified by statistical theories such as RRKM theory, which is commonly called the quasi-equilibrium theory (QET) for dissociation of a molecular ion [3]. Such theories assume *a priori* the existence of a bound and stable ground state of the molecular ion. However, in many of the ions described in this paper (e.g. CF_4^+) the ground state of the molecular ion is not bound in the Franck-Condon region, and secondly it appears that many of such-sized ions do not possess a high enough density of states to belong to the 'large molecule' limit. Under these circumstances, dynamical rather than statistical dissociation properties are observed.

Two experiments utilising tunable VUV radiation from a synchrotron are used to measure some of the dynamical decay properties of excited states of MX_n^+. Radiative decay is measured in a crossed gas spray−tunable VUV beam apparatus with undispersed fluorescence detection [4]; in more recent experiments [5] it has proved possible to disperse the fluorescence through a small monochromator, yielding low-resolution electronic spectra of the emitting molecular ion. These experiments started in 1987 at the Daresbury source in the UK, and continue both there and at the BESSY 1 source in Berlin. The results of the earlier experiments were reviewed in 1990 [6]. In these experiments thresholds for fluorescence are determined, and in favourable cases an estimate of the fluorescence quantum yield, Φ_F, or (more accurately) radiative probability of the excited electronic state of MX_n^+ can be made. Furthermore, the shape of the peaks in the fluorescence excitation spectrum can inform whether the emission is due to an excited state of the parent ion of MX_n or due to a neutral fragment [6]. Using the synchrotron in its pulsed mode, lifetimes, τ, of the emitting states can also be measured very accurately. Since $\Phi_F = k_{rad}/(k_{rad} + k_{non\text{-}rad})$ and $\tau^{-1} = (k_{rad} + k_{non\text{-}rad})$, changes in Φ_F and τ with excitation energy are especially revealing since they may be attributed to a change in $k_{non\text{-}rad}$, i.e. the onset of a competitive, non-radiative channel. However, the fragment ions produced by such a process are not probed directly. Furthermore, these radiative experiments are not state-selected, because at any photon energy a range of vibronic levels of $MX_n^{+(*)}$ will be produced in the Franck-Condon region, since at no point is the energy of the emitted photoelectron measured or defined.

State-selected, non-radiative decay dynamics of vibronic states of $MX_n^{+(*)}$ are made in a recently-constructed coincidence apparatus [7] which incorporates a threshold electron analyser and a time-of-flight (TOF) mass spectrometer, allowing the fragmentation of $MX_n^{+(*)}$ to be measured over a range of photon energies and hence valence electronic states by TPEPICO spectroscopy. Note that this is the predicted decay channel for a statistical dissociation of the parent ion in the large-molecule limit. The very recent addition of a fast photomultiplier tube for the detection of undispersed fluorescence [8] allows the two types of coincidence experiment involving photon emission (PIFCO and TPEFCO) also to be made, allowing us to study in intimate detail the competition between radiative and non-radiative decay in isolated states of polyatomic ions. These experiments started in 1991, and the purpose of this paper is to review the results we have obtained to date with this apparatus.

2. Experimental

Our first attempts to measure non-radiative decay dynamics of polyatomic ions were only partially successful, in that we employed an electron−ion

coincidence technique in which *all* electrons with energies from zero to ca. 8 eV were collected with high efficiency [9]. Ions were collected by TOF mass spectrometry. The apparatus consisted of two identical TOF drift tubes (field-free region 70 mm long) for the detection of electrons and ions. An extraction field of 80 V cm^{-1} accelerated electrons into one tube, ions into the other, and the two signals were detected by a time-correlated coincidence technique. Repeated as a continuous function of photon energy, such experiments measured thresholds for fragment ion production and ion yield curves in a number of molecular systems (e.g. CF_4 and CCl_4 [9], CF_3Cl and CF_3Br [10], BF_3 and BCl_3 [11], and SF_6 [12]). The data obtained was thus very similar to that obtained from photoionisation mass spectrometry. However, the principal limitation of this apparatus, easy to see with the benefit of hindsight, was that there was no energy analysis of the photoelectrons, and they were in effect used only to provide the 'start' signal for the coincidence experiment. Electrons therefore originated from photoionisation of MX_n to many vibronic states of the parent ion, making this a non-state-selected experiment. Measurement of the translational KE release in a dissociative ionisation process was possible, but interpretation of the data was almost meaningless. These experiments, performed between 1988 and 1991, were reviewed elsewhere [6].

The use of a threshold, or zero-energy electron analyser is ideal to provide the discrimination against energetic electrons produced from lower-lying electronic states of MX_n^+ or autoionising states of the neutral molecule. Our new apparatus is shown in Fig. 1. It incorporates a threshold electron analyser, a TOF mass spectrometer, and a fast photomultiplier tube for photon detection. In principle, the apparatus can be attached to any VUV beamline at any synchrotron; in practice, to date we have only used the 1 m Seya and the 5 m McPherson VUV beamlines at the Daresbury source. The different parts of the apparatus are now described in detail.

2.1 The threshold electron analyser

Three techniques are commonly used to detect threshold electrons in a continuous or c.w. apparatus; high-resolution dispersive analysis [13], steradiancy analysis [14], and low extraction field analysis [15]. The first of these methods suffers from low collection efficiency due to the small solid angle subtended. Steradiancy analysis, in which electrons are accelerated into a field-free region consisting of a tube or collimated hole array with a large length-to-diameter ratio, can achieve high efficiency, but a major drawback is that energetic electrons ejected parallel to the axis are also detected, giving rise to the 'high-energy tail' in the transmission function. Such electrons can be removed either by timing techniques (needing single-bunch mode of the synchrotron [16]) or with a dispersive post-analyser, but since steradiancy analysers do not focus the electrons the overall efficiency

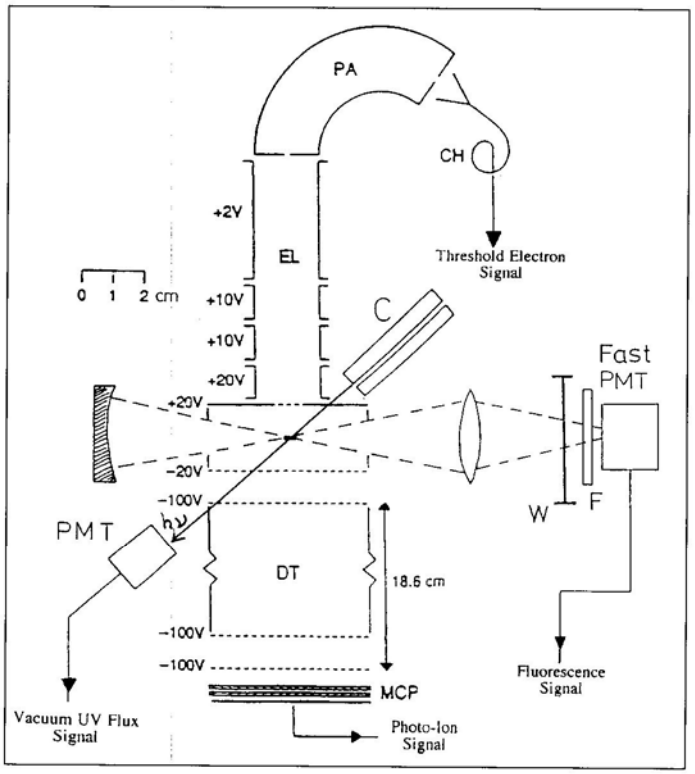

Fig. 1. Schematic of the apparatus which can perform TPEPICO, PIFCO and TPEFCO coincidence spectroscopies. EL, electron lens; PA, post analyser; CH, channeltron electron multiplier; C, capillary; W, window; F, filter; DT, drift tube; MCP, multi-channel plates; PMT, photomultiplier tube.

is reduced. In the low extraction field analyser low-energy electrons are extracted from the interaction region by a weak penetrating field (typically a few meV cm^{-1}) from an external electrode. The configuration of the field is such that only threshold electrons focus at the centre of a small post-analyser. High collection efficiencies and resolution (half-widths down to 2 meV) have been achieved [15]. Our analyser (Fig. 1) combines properties of both the steradiancy and the penetrating-field detectors. We use an electrostatic lens designed with large chromatic aberrations followed by a small 127° post-analyser. Primary filtering is provided by the lens so that only low-energy electrons focus at the 2 mm diameter entrance to the post-analyser. Even with an extraction field as large as 20 V cm^{-1}, simulations have predicted [7] and experiments have confirmed [17] that the analyser has both a high collection efficiency (ca. 30% for zero-energy electrons) and

good resolution (ca. 4 meV half-width). This is not the most efficient threshold analyser that can be built. However, we believe that it is an effective compromise for a TPEPICO experiment in which the coincidence rate is proportional to the *product* of the collection efficiencies of electrons and ions, and a high extraction field is desirable in the interaction region for an ion TOF drift tube, especially if energetic ions are present.

2.2 The time-of-flight mass spectrometer

The ion detector consists of a linear TOF drift tube configured to satisfy spatial focussing [18]. Like the threshold electrons, ions are extracted by a field of 20 V cm $^{-1}$, further accelerated to a potential of -96 V, pass down the field-free region (length 186 mm), and detected by a pair of microchannel plates. The (large) extraction field of 20 V cm^{-1} is needed for high ion collection efficiency, and a consequence of spatial focussing is that the TOF of the ion is proportional to the component of the momentum along the axis for initial energies up to ca. 10% of the potential applied to the field-free region (in this apparatus ca. 9 eV). This allows the measurement of a KE release from a dissociative ionisation process whilst still retaining a high collection efficiency. Although TPEPICO experiments have been performed for diatomic ions with the penetrating field analyser using an extraction field for ions of only a few meV cm^{-1} [15], we do not believe that this can be a general technique for the measurement of KE releases in dissociative processes in state-selected polyatomic ions, and we rejected this form of analyser in our design.

2.3 Fluorescence detection

Fluorescence from the interaction region orthogonal to the direction of the electron and ion flight tubes is collected by an *f*/1 biconvex quartz lens of focal length 50 mm and detected by a photon-counting photomultiplier tube (PMT) cooled to 253 K. For most of the experiments a fast Mullard 2254 QB (risetime 1.5 ns), red-sensitive tube (wavelength range 200–750 nm) was used. An *f*/1 concave mirror of focal length 75 mm placed behind the interaction region enhances photon collection efficiency. We comment that the fluorescence optics were added at a later stage to the original design of the apparatus which was optimised specifically for TPEPICO experiments. Therefore the photon collection efficiency is not as high as it could be in an apparatus optimised for PIFCO and TPEFCO fluorescence coincidence experiments.

2.4 Photon sources flux normalisation and gas inlet

Synchrotron radiation is dispersed either using a 1 m Seya-Namioka (in this paper abbreviated to Seya) or a 5 m normal-incidence McPherson mono-

chromator. Both cover the wavelength range 40−120 nm or ca. 10−30 eV with an ultimate resolution in the scanning mode of 0.05 and 0.015 nm, respectively. The dispersed VUV radiation enters a stainless-steel chamber via a 100 mm long, 2 mm internal diameter glass capillary, and is monitored by a sodium-salicylate-coated window and a photomultiplier tube which allows for flux normalisation of the data. The glass capillary provides both collimation of the beam and differential pumping between the monochromator and the experimental chamber. The molecule under study effuses through a 0.5 mm internal diameter stainless-steel needle whose tip is located ca. 25 mm from the centre of the interaction region. Under these circumstances, there is no axial or translational cooling of the molecules and a temperature of 300 K is assumed.

2.5 Data accumulation

The raw pulses from the electron, ion and photon detectors are passed to discriminator and pulse-shaping circuits, and any two of them are passed into a time-to-digital converter (TDC, LeCroy 4208) configured in the multi-hit mode. One provides the start pulses, the other the stop pulses, hence the two signals from the same ionisation event are detected in time-delayed coincidence. Interchange between the three different forms of coincidence experiment is trivial, and in theory data from each of the three experiments can be collected either at a fixed photon energy, or continuously, flux normalised, as a function of photon energy. The scanning of the VUV monochromator and the collection of the coincidence data are controlled by two IBM personal computers which interact through CAMAC-based electronics. Full details are given elsewhere [7].

3. Coincidence spectroscopies and experimental techniques

The information that can be obtained from the three different forms of coincidence experiment (TPEPICO, PIFCO and TPEFCO) is varied and complementary. TPEPICO spectroscopy allows the fragmentation channels of both ground and excited electronic states of ions to be studied, and these measurements can often be made with vibrational resolution in the parent ion. The fragment ions that are observed, and the KE released into these ions, are important guides to statistical or dynamical behaviour in the ion. PIFCO spectroscopy can be used to determine whether an excited state of a molecular ion decays by a radiative process. If coincidences are observed, with sufficient time resolution it is possible to measure the lifetime, τ, and quantum yield, Φ_F, of the fluorescing state of the ion, but because the energy of the ejected photoelectron is not defined, these quantities are averaged over the Franck-Condon populations of the vibrational levels of the

fluorescing state. By observing the mass of the ion which is detected in coincidence with the photon, the fate of the lower electronic state to which fluorescence occurs can be determined. The TPEFCO technique can also determine τ and Φ_F, but now the resolution is determined by that of the photoionising beam and the electron analyser. In this way, vibrational state-selectivity can be achieved. Changes of $(\Phi_F)_v$ and τ_v with vibrational level (v) are the most interesting because they can often be attributed to a change in $k_{\text{non-rad}}$, i.e. the onset of a competing non-radiative channel. Such a situation arises for the different v_1 vibrational levels of the $\tilde{C}\ ^2T_2$ excited valence state of CF_4^+ (Section 5.2). If the ion under study is approaching the large-molecule limit, then the observation of a PIFCO or TPEFCO spectrum, and hence the presence of radiative decay in an excited state of the ion, can be regarded as one manifestation of non-statistical bchaviour.

We stress the versatility of the apparatus which can perform the following experiments. First, a threshold photoelectron spectrum (TPES) of the sample gas can be recorded, and this experiment is always performed as a precursor to the coincidence experiments. By this method we calibrate either monochromator over its complete range using well-established energies of vibrational levels of O_2^+ X $^2\Pi_g$ around 12 eV, of B $^2\Sigma_g^-$ around 20 eV, and of c $^4\Sigma_u^-$ around 25 eV [19]. The major interest in a TPES of a polyatomic molecule is to see how it differs from the spectrum obtained with He I (21.22 eV) and/or He II (40.8 eV) fixed-energy line sources. Anomalous intensity effects in the TPES are often due to autoionisation which is known to produce non-Franck-Condon vibrational distributions, caused by autoionisation of high Rydberg states of the neutral molecule competing with direct Franck-Condon ionisation. Second, TPEPICO, PIFCO and TPEFCO coincidence spectra can be recorded at a fixed photon energy. In a TPEPICO spectrum of this kind, to obtain the kinetic energy release distribution (or KERD) [20], TOF data accumulate at as high a time resolution of the TDC as the signal level will permit. In PIFCO and TPEFCO spectra of this kind, coincidence count rates are much lower, primarily because of the inferior collection efficiency of photons compared to ions or electrons, and time resolution is then sacrificed to obtain a spectrum in a reasonable period of time. Thus, we do not measure lifetimes with the PIFCO experiment but use it solely to determine whether an excited state of a molecular ion fluoresces, and if so which ion is observed in coincidence with the photon. In a TPEFCO spectrum the electrons provide the start, the fluorescent photons the stop pulses. The time resolution of this experiment is limited by that of the TDC, in our case 1 ns, and we use this experiment to measure lifetimes of (where possible, vibrationally-state-selected) fluorescing ions. Third, a TPEPICO spectrum can be recorded continuously as a function of photon energy. Usually all the ions produced in the TPEPICO spectrum are recorded in this energy-scanning mode, and the resolution of the TDC is correspondingly degraded. Data accumulate as a three-dimen-

sional histogram of photon energy vs. ion TOF vs. coincidences. The total electron count is also recorded, so a two-dimensional representation of the threshold photoelectron spectrum and the yields of all the fragment ions can be generated from the raw data. This is the way the data is presented, because in non-statistical processes the yields of daughter ions generally correlate with different electronic states of the parent ion. Breakdown diagrams [21] show which daughter ions dominate at each photon energy, and are less instructive for non-statistical fragmentation pathways. Although possible, we do not perform the PIFCO and TPEFCO experiments in this energy-scanning mode.

All the coincidence experiments operate in the multi-bunch, quasi-c.w. mode of the synchrotron source (160 bunches of electrons, width 0.2 ns, 2 ns between bunches in the storage ring), and pulsed extraction using the single-bunch mode is not used for either electron or ion detection. In this way we utilise the limited beam time allocated on the synchrotron source to its optimum. Furthermore, because the flight time of the photoelectron which provides the start signals is accurate to ± 3 ns, this mode of operation places very few limitations either on the resolution of TOF spectra that are measured by the TPEPICO technique or on the lifetime of an emitting ionic state that can be measured by the TPEFCO technique. Deconvolution of this effect in TPEFCO spectra is only really desirable for $\tau \leq$ ca. 5 ns, and has not been performed in any of the spectra studied to date.

4. Analysis of the Kinetic Energy Release Distributions: statistical vs. impulsive dissociation

The analysis of the KE information from the fixed-energy TPEPICO spectra warrants some discussion, because the results of these experiments are one criterion to establish statistical or non-statistical behaviour in an electronic state of a polyatomic ion. Fig. 2 shows the broadening of the CF_3^+ and CF_2^+ peaks, both produced from photoionisation of CF_4 into the $\tilde{C}\ ^2T_2$ ionic state at an energy close to the Franck-Condon maximum. Interpretation of the results is given in Section 5. Here we concentrate on how the mean translational KE release, $\langle KE \rangle_t$, is determined. Analytical expressions [22] are available for obtaining $\langle KE \rangle_t$ from such peaks, however assumptions have to be made about the overall shape of the peak. We use the method developed by Powis *et al.* [20] to extract a *distribution* of KE releases and hence $\langle KE \rangle_t$. This method makes no initial assumption about the overall peak shape. A set of TOF peaks, each with a discrete energy release, ε_t is calculated. The number of components and the energy, ΔE, of the first member of the set depend primarily on the statistical quality of the data. The discrete energies are given by $\varepsilon_t = (2n-1)^2 \Delta E$ where $n = 1,2,3,\ldots$. A Gaussian tail is added to each rectangular TOF peak to allow for the effects

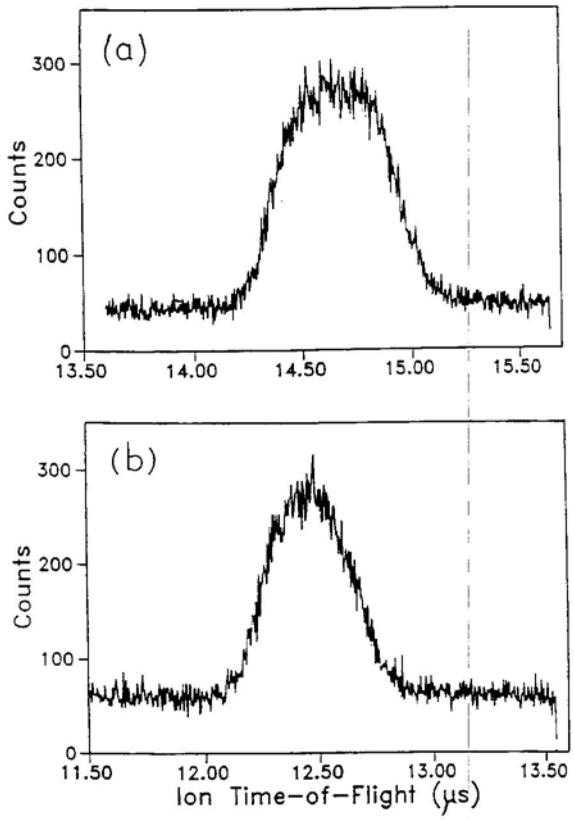

Fig. 2. Coincidence time-of-flight spectrum of (a) CF_3^+, and (b) CF_2^+ from CF_4 excited at 22.2 and 22.5 eV, respectively, into the $\tilde{C}\ ^2T_2$ ionic state. In both spectra, the time resolution is 4 ns per channel. Analysis of the peak shape using the method of Powis [20] yields $\langle KE \rangle_t$ values of 1.34 ± 0.10 and 0.57 ± 0.06 eV, respectively.

of thermal broadening. The set of computed TOF peaks are obtained by performing Monte-Carlo trajectory calculations of ions through the TOF mass spectrometer. Inputs to the program indude the masses of the parent and daughter ions, the geometry of the mass spectrometer, and the translational temperature of the parent ion both along and perpendicular to the axis of the apparatus. The co-added TOF peaks are then fitted to the experimental peak using a linear regression technique. Outputs are the normalised probability distributions of ε_t and hence $\langle KE \rangle_t$. In this way we determine $\langle KE \rangle_t$ values of 1.34 ± 0.10 and 0.57 ± 0.06 eV for Figs. 2(a) and (b), respectively. Note that for the CF_2^+ channel, a two-body process with F_2 as the neutral product is assumed. In theory, the position of the peak in the

$P(\varepsilon_t)$ vs. ε_t graph can also give information on the statistical or non-statistical nature of the dissociation process, with non-statistical processes exhibiting a maximum at larger values of ε_t than statistical processes. In practice, we do not interpret the distribution graphs in more detail due to the lack of cooling of the translational temperature, T, of molecules along the axis of the TPEPICO apparatus, since molecules emerge from the inlet needle with little or no directionality. With $k_B T$, as high as 25 meV, this thermal effect degrades the detailed form of the TOF distribution, and allows only mean KE releases to be obtained with reliable accuracy.

For dissociation of a polyatomic ion to a daughter ion plus atom, we can use the values of $\langle KE \rangle_t$ to determine whether dissociation is essentially a statistical or an impulsive, dynamical process. Consider a general photodissociation from $ABC^{+(*)} \rightarrow AB^+ + C$ where AB^+ represents a polyatomic fragment (e.g. CF_3^+) and C an atom. There are two limiting extremes for such a process. In one extreme, the photoexcited parent ion is long-lived on the time period of rotational and vibrational internal motion so that any excess energy is partitioned statistically amongst the available degrees of freedom prior to dissociation. In this instance a relatively small amount of the excess energy is partitioned into translational motion of the products (the property we measure in our experiments), with the majority being partitioned into internal energy of AB^+. As a general rule, $\langle KE \rangle_t$ decreases as the mass or complexity of the polyatomic ion AB^+ increases. In the other extreme, $ABC^{+(*)}$ is so short-lived that dissociation occurs on a time scale which is comparable to or faster than that of internal molecular motion. Now a much greater fraction of the excess energy is partitioned into translational KE of the $AB^+ + C$ products. These two extremes are called statistical [23] and impulsive [24] photodissociation. In the former case, RRKM or QET can be used to calculate dissociation rates, and, as mentioned in Section 1, the details of the electronic state to which ABC is initially photoionised are usually not important because internal conversion to the ground state is assumed to take place so rapidly that dissociation only occurs from this surface. In the latter case, dynamical or impulsive theories can be used to calculate energy releases, and now the detailed topography of the potential energy surface(s) from which dissociation occurs is crucial to interpret the dynamics.

Klots [25] has shown that for a statistical dissociation in which both energy and angular momentum are conserved, and where the excess or available energy is large enough that any activation or centrifugal barrier in the exit channel to dissociation products can be neglected, then E_{avail} and $\langle KE \rangle_t$ are related by a simple analytical expression:

$$E_{avail} = \frac{(r-1)}{2}\langle KE \rangle_t + \langle KE \rangle_t + \sum_i \frac{h\nu_i}{\exp\left(\frac{h\nu_i}{\langle KE \rangle_t}\right) - 1} \qquad (3)$$

E_{avail} is given by the photon energy minus the energy of the $AB^+ + C$ dissociation channel, r is the number of rotational degrees of freedom of AB^+, and ν_i are the vibrational frequencies of the AB^+ fragment. For $CF_4^+ \rightarrow CF_3^+ + F$ excess energies are typically greater than 1 eV, centrifugal barriers are small for long-range ion-induced dipole (Langevin) interactions [23], therefore the approximations of Klots are valid and Eq. (3) can be applied to such dissociation processes. Conversely, for an impulsive dissociation Riley and Wilson [24] have shown that E_{avail} and $\langle KE \rangle_t$ are related by:

$$\frac{\langle KE \rangle_t}{E_{avail}} = \text{Fraction}_{impulse} = \frac{\mu_{A,B}}{\mu_{AB,C}} \tag{4}$$

where μ is a reduced mass. In this way greater fractions of E_{avail} are channelled into translational energy of the products than the fractions calculated by phase-space methods [25]. For the photodissociation processes observed involving loss of a halogen atom, we compare the experimental fraction of the available energy channelled into translational energy of products with that calculated by these two limiting models (Sections 5.2 and 5.3). In this way we can make some general statements about the nature of the photodissociation dynamics of state-selected electronic states of halogenated molecular ions.

5. Results

We have performed experiments on a range of polyatomic molecules; the tetrahalides and mixed halides of group 4 (e.g. CF_4 and SiF_4 [17], CCl_4, $SiCl_4$ and $GeCl_4$ [17, 26], CF_3Cl and CF_3Br [10]), BCl_3 [27] and SF_6 [28]. Most detailed work has been performed on CF_4^+, and we highlight these results in this paper (Sections 5.1 and 5.2). In Section 5.3 we show that many of the excited states of CF_3Cl^+ and CF_3Br^+ show non-statistical decay pathways. Finally, in Section 5.4 we comment on some interesting aspects of the fluorescence coincidence experiments, with particular reference to the $\tilde{C}\ ^2T_2$ state of $SiCl_4^+$ and the $\tilde{D}\ ^2E'$ state of BCl_3^+.

5.1 The group IV tetrahalide molecular ions (e.g. CF_4^+): non-state-selected fluorescence experiments

The simplest member of this family, CF_4^+, shows many of the properties of non-statistical decay from nearly all its outer-valence electronic states, and is therefore a prototypical ion to study by coincidence techniques. The electronic configuration of the five highest molecular orbitals of CF_4 is $\ldots(2a_1)^2(2t_2)^6(1e)^4(3t_2)^6(1t_1)^6$, and potential energy curves for the ground and first four excited states of CF_4^+ are shown in Fig. 3. Also shown are the energies of the lowest dissociation channels to fragment ions such as CF_3^+

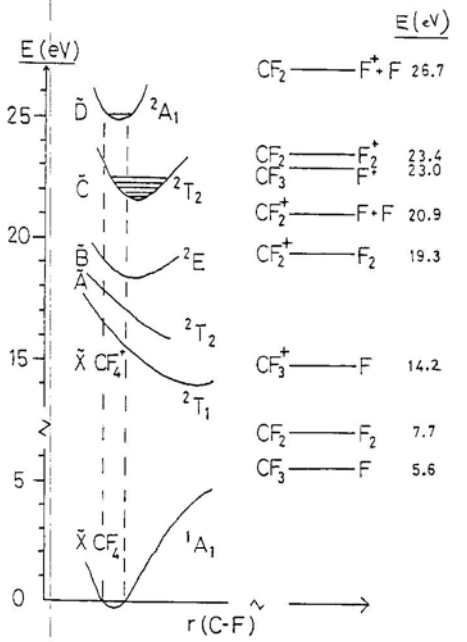

Fig. 3. Potential energy curves of the valence states of CF_4^+ and the lowest dissociation energies of the fragment ions.

and CF_2^+, these values being calculated from heats of formation and adiabatic ionisation potentials (IP) of the neutral fragments. Details can be found elsewhere [17]. Note that due to the relatively high value of the IP(CF_4) and low value of the IP(CF_3), the ground state of CF_4^+ in the Franck-Condon region lies *above* the energy of CF_3^+ + F and is therefore a repulsive state. Note also the presence of bound, excited states of the parent ion ($\tilde{C}$ $^2T_2$ and $\tilde{D}$ $^2A_1$) which can support vibrational and rotational levels and which lie above several dissociation channels. This is a surprising phenomenon in a polyatomic ion comprised of five 'heavy' atoms. Only the three highest molecular orbitals of CF_4 are accessible with He I radiation. He I and He II photoelectron spectra were reported in the 1970s [29], and recently spectra recorded under threshold conditions have been reported both by Yencha *et al.* [30] and by us [17]. The first two bands correspond to electron removal from F 2pπ non-bonding orbitals and ionisation to the $\tilde{X}$ $^2T_1$ and $\tilde{A}$ $^2T_2$ states. Both these repulsive states dissociate adiabatically to CF_3^+ + F. No vibrational structure is observed, showing that dissociation is fast, probably on a sub-ps timescale (i.e. a non-statistical process). The third band (ionisation from another F 2pπ non-bonding orbital to $\tilde{B}$ ^2E) shows a partially-resolved progression in ν_1 (810 cm^{-1}) and possibly ν_2 (400 cm^{-1}), the latter

presumably arising from Jahn-Teller distortion of the state from T_d symmetry. The third and fourth bands arise from electron removal from C-F σ-bonding $2t_2$ and $2a_1$ molecular orbitals, and show extended vibrational progression in ν_1 (729 and 800 cm^{-1} in $\tilde{C}\ ^2T_2$ and $\tilde{D}\ ^2A_1$, respectively [31]). In the latter case the long progression is only observed under threshold electron conditions [17, 30], and therefore arises due to autoionisation from high-lying Rydberg states of CF_4 around 25 eV.

The presence of discrete structure in the photoelectron spectra suggests that the $\tilde{C}$ and $\tilde{D}$ excited states of CF_4^+ are relatively long-lived and may fluoresce, and both these states do indeed show radiative decay with lifetimes of ca. 9 and 2 ns respectively [32]. Note that since fragmentation of these states to CF_3^+ and CF_2^+ is energetically allowed, the observation of fluorescence represents one manifestation of non-statistical behaviour. Initial experiments on the spectroscopic properties of these excited states of CF_4^+ were made at Birmingham in a crossed supersonic beam – electron beam apparatus with dispersed fluorescence detection [31]. Both bound-bound, discrete (e.g. $\tilde{D}$-$\tilde{C}$) and bound-free, continuous (e.g. $\tilde{D}$-$\tilde{A}$, $\tilde{C}$-$\tilde{A}$, $\tilde{C}$-$\tilde{X}$) spectra were observed rotationally cooled to ca. 25 K. Analysis of the rotational envelope of vibronic bands of the bound-bound $\tilde{D}\ ^2A_1$–$\tilde{C}\ ^2T_2$ transition allowed spectroscopic constants (e.g. rotational constants, Coriolis and spin-orbit splitting constants in the triply-degenerate $\tilde{C}$ state) to be determined [33]. However, other than confirming that any Jahn-Teller distortion of the $\tilde{C}\ ^2T_2$ state from tetrahedral geometry was negligible, these experiments gave essentially no information on the dynamical properties of these excited states. For example, what are the lifetimes, do they change with vibrational quantum number, does fluorescence from the $\tilde{C}$ and $\tilde{D}$ states of CF_4^+ represent a major or a minor decay channel, and if a minor channel what are the fragment ions produced by the competing non-radiative pathway and what are the KE releases in the fragmentations?

Our first dynamical experiments at Daresbury studied the radiative decay properties of such excited states of CF_4^+ by VUV fluorescence excitation spectroscopy [4]. An effusive flow of gas is crossed orthogonally by tunable VUV radiation, and fluorescence is observed undispersed at right angles to both the gas flow and the direction of the VUV beam. Since the excitation source is linearly polarised, the fluorescence may show alignment effects which give information on how the ionising electron is ejected into the different continuum channels. To date, we have not explored such effects in detail. To maximise photon collection efficiency, we observe fluorescence at right angles to the photon flux, and not at the magic angle where alignment effects are not important. Fig. 4 shows the spectrum when CF_4 is excited by photons in the range 21–30 eV. In (a) an EMI bi-alkali photomultiplier tube is filtered so that photons in the range 250–390 nm only are collected; this encompasses most of the bound-free $\tilde{C}$-$\tilde{A}$ and $\tilde{C}$-$\tilde{X}$ transitions in CF_4^+. In (b) a solar-blind tube (collecting $120 < \lambda < 200$ nm) is used;

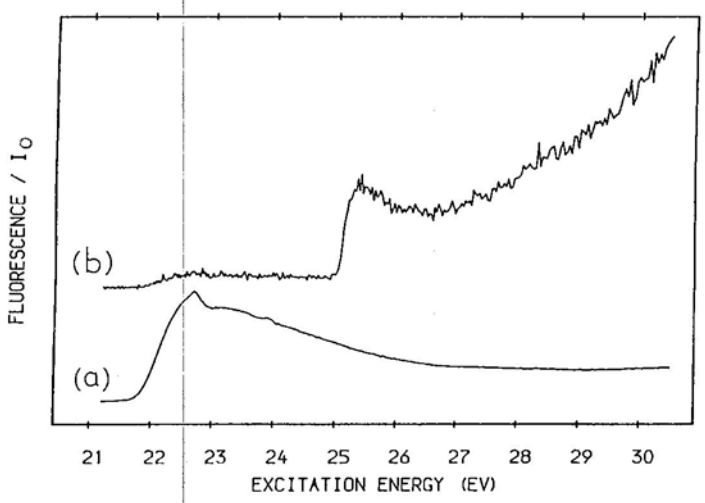

Fig. 4. Undispersed fluorescence from CF_4 excited by vacuum-UV radiation in the range 21−30 eV at a resolution of 0.2 nm or ca. 0.1 eV. In (a) UV fluorescence in the range 250−390 nm is collected, in (b) only vacuum-UV fluorescence in the range 120−200 nm is collected. The photon signals have been normalised to the synchroton flux, I_0. The scale of the normalised fluorescence axis is different in the two spectra. (Reproduced by permission from J. Chem. Phys. **89** (1988) 2683).

this encompasses most of the bound-free $\tilde{D}$-$\tilde{A}$ and $\tilde{D}$-$\tilde{B}$ transitions in CF_4^+. Thresholds are observed at 21.7 ± 0.1 and 25.0 ± 0.1 eV, in excellent agreement with the adiabatic IPs of the $\tilde{C}$ and $\tilde{D}$ states of CF_4^+ [17, 29, 30]. These spectra show two important characteristics of a photoionisation process. First, the steepness of the 'turn on' is governed by ionisation Franck-Condon factors. Fig. 4(b) shows a steep rise at threshold because ionisation to $\tilde{D}\ ^2A_1$ is a near-vertical process with little change in molecular geometry, whereas the rise in Fig. 4(a) is more gradual because ionisation to $\tilde{C}\ ^2T_2$ involves a substantial increase (0.08 Å) in the C−F bond distance [33]. Second, the fluorescence signal remains non-zero for photon energies well in excess of threshold. This arises because photoionisation is a non-resonant process since the electron can carry away the excess energy. The intensity of the emission is then determined primarily by the variation of the partial ionisation cross-section for the ionic state under study with energy.

If such cross-sections are known from angle-resolved photoelectron spectroscopy, from the intensity of the fluorescence signal it is possible to estimate the quantum yield, Φ_F, of the fluorescing ionic state. This measurement has been possible for the CF_4^+ $\tilde{C}$ state, both because values for σ_C are known [34] and because the bi-alkali tube which detects CF_4^+ $\tilde{C}$-$\tilde{A}$,$\tilde{X}$ emission can also detect N_2^+ B-X emission. Hence it has been possible to calibrate the photon collection efficiency of the apparatus with N_2^+ for which

Table 1. Lifetime, τ, of CF_4^+ $\tilde{C}\ ^2T_2$ as a function of excitation energy, E, as measured by time-resolved fluorescence[a].

λ/nm	E/eV	τ/ns[b]
56.5	21.9	9.66 ± 0.05
55.5	22.3	9.35 ± 0.05
54.5	22.7	8.75 ± 0.03
52.5	23.6	8.58 ± 0.02
50.5	24.5	8.61 ± 0.03
48.5	25.6	8.59 ± 0.03
46.5	26.6	8.65 ± 0.03
44.5	27.8	8.84 ± 0.05
42.5	29.2	8.96 ± 0.05

[a] Taken from Reference [4].
[b] The error represents one standard deviation of the fit.

all the decay properties of the B state are known. The procedure is described elsewhere [4]. We obtain $\Phi_F = 0.5 \pm 0.4$ at the peak of the excitation spectrum (22.6 eV), suggesting that a competing non-radiative channel is operative. Note that this is *not* a state-selected value of Φ_F at this energy, but a valve appropriate for a Franck-Condon-weighted average of the vibrational levels of CF_4^+ $\tilde{C}$ between threshold (21.7 eV) and 22.6 eV which are populated by photoionisation. Note also that we believe that the error in Φ_F through not detecting fluorescence at the magic angle to the E-vector of the VUV incident radiation is minimal compared to other errors which arise in a quantitative determination of Φ_F of this kind. Measurements of Φ_F by this method are both rare and difficult since partial ionisation cross-sections are known only for relatively few of the polyatomic molecules we have studied, and the photomultiplier tube has to be sensitive to radiation at 390 nm to calibrate with N_2^+ B-X emission. For this reason it was not possible to estimate Φ_F for the $\tilde{D}\ ^2A_1$ state of CF_4^+.

Another indicator that the fluorescence quantum yield of the $\tilde{C}\ ^2T_2$ state of CF_4^+ is not its maximum value of unity comes from measurements of the lifetime, τ, using the single-bunch mode of the synchrotron. With a pulse width of 0.2 ns and a flight time around the ring of 320 ns, the Daresbury source can be used to measure lifetimes in the range 1−100 ns with a high degree of precision. Lifetimes outside this range (especially small values) can be measured, but careful deconvolution techniques for the excitation pulse need to be used. Data accumulate rapidly due to the 3 MHz repetition rate so that experiments are performed relatively quickly. Table 1 shows the lifetime of the CF_4^+ $\tilde{C}$ state measured by this technique at excitation energies between 21.9 eV (just above threshold) and 29.2 eV. The lifetime decreases from 9.7 ns at threshold to a minimum of 8.6 ns 4 eV above threshold, then rises again to 9.0 ns at 29.2 eV [4]. Again, note that these are *not* state-

selected lifetimes for the same reason as given above. Since $\tau = (k_{rad} + k_{non\text{-}rad})^{-1}$ changes of τ with photon energy could be due to a change of k_{rad} with energy, the presence of a non-radiative decay channel, or both. For a bound-bound transition k_{rad} from a defined v' level of a fluorescing state is given by

$$(k_{rad})_{v'} = \sum_{v''} A_{v',v''} = \frac{R_e^2 \cdot \sum_{v''} (\nu^3)_{v',v''} q_{v',v''}}{4.94 \times 10^5} \text{ s}^{-1} . \quad (5)$$

$A_{v',v''}$ is the Einstein A-factor, R_e the electronic transition moment (in atomic units), $\nu_{v',v''}$ the energy of a $v' \rightarrow v''$ vibronic transition (in cm^{-1}) and $q_{v',v''}$ its corresponding Franck-Condon factor [35]. As v' increases (corresponding in our experiment to an increase in photon energy), it is not always obvious whether $(k_{rad})_{v'}$ increases or decreases, and for a bound-free transition (e.g. CF_4^+ $\tilde{C}$-$\tilde{A}$ and $\tilde{C}$-$\tilde{X}$) it is certainly not clear how k_{rad} will change with increasing photon energy. However, given that the multi-bunch experiment established that Φ_F is probably less than unity, coupled with these lifetime results, the data suggest that the $\tilde{C}$ $^2T_2$ state of CF_4^+ does decay by a non-radiative process which is in competition with fluorescence. Furthermore, it seems that different values of $k_{non\text{-}rad}$ pertain to different vibrational levels of the $\tilde{C}$-state parent ion. We have therefore studied this state in detail using the three coincidence techniques described in Section 3.

5.2 Coincidence experiments on the valence electronic states of CF_4^+

We have now performed three kinds of electron-ion coincidence experiment on the valence states of CF_4^+. First, using the Seya monochromator and the original non-state-selected apparatus [9], electron-ion coincidence spectra were recorded as a function of photon energy over the range 15−27 eV. CF_3^+ and CF_2^+ were the only ions observed (the raw data collected as a three-dimensional false-colour map of photon energy vs. ion TOF vs. coincidence is shown in Fig. 12 of [6]), and their ion yields and thresholds for production obtained. Thresholds of 15.8 ± 0.1 and 21.7 ± 0.2 eV respectively were measured. Note that these values are substantially higher than the lowest thermochemical thresholds for production of these ions [14.2 and 19.3 eV respectively (Fig. 3)]. The measured values correspond approximately to the adiabatic IP of the $\tilde{X}$ $^2T_1$ and $\tilde{C}$ $^2T_2$ states of CF_4^+, hence this result suggests that CF_4^+ $\tilde{C}$ shows non-radiative decay to CF_2^+. However, due to the lack of an electron energy analyser in this apparatus, it was not possible to say whether the fragmentation channels observed at the energies of each of the five outer-valence electronic states of CF_4^+ were unique. Second, again using the Seya but now with the new coincidence apparatus, TPEPICO spectra were recorded over the same range of photon energies at a moderate resolution of ca. 0.1 eV [28]. KERDs were also measured at the

Table 2. Mean translational KE release, $\langle KE \rangle_t$, from fragmentation of valence states of  .

Daughter Ion	Parent Ion	Electronic State	Energy/eV	$\langle KE \rangle_t$/eV[b]
CF_3^+	CF_4^+	$\tilde{X}\ ^2T_1$	16.3	0.97 ± 0.05
CF_3^+	CF_4^+	$\tilde{A}\ ^2T_2$	17.5	1.19 ± 0.04
CF_3^+	CF_4^+	$\tilde{B}\ ^2E$	18.6	1.27 ± 0.14
CF_3^+	CF_4^+	$\tilde{C}\ ^2T_2$	22.2	1.34 ± 0.10
CF_2^+	CF_4^+	$\tilde{C}\ ^2T_2$	22.5	0.57 ± 0.06[c]
CF_3^+	CF_4^+	$\tilde{D}\ ^2A_1$	25.3	1.54 ± 0.13
CF_2^+	CF_4^+	$\tilde{D}\ ^2A_1$	25.3	1.50 ± 0.26[c]

[a] Taken from Ref. [28].
[b] The error quoted is one standard deviation of the fit. It is probably an underestimate of the experimental uncertainty.
[c] Assumes the other product is F_2.

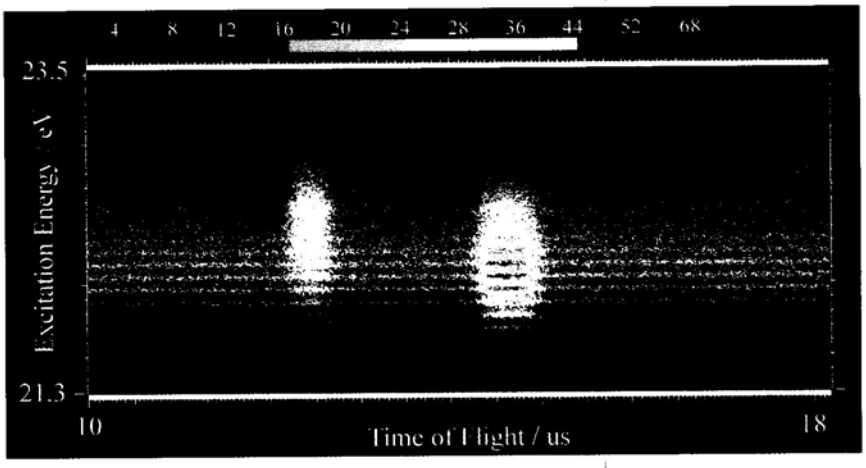

Fig. 5. False-colour coincidence map of fragmentation of the $\tilde{C}\ ^2T_2$ state of CF_4^+ recorded at a resolution of 0.05 nm or ca. 0.02 eV. The signals centred at time-of-flights of 12.5 and 14.6 μs correspond to CF_2^+ and CF_3^+, respectively.

Franck-Condon maxima of the five states of CF_4^+, and $\langle KE \rangle_t$ values determined. The results are shown in Table 2. As expected, the $\tilde{X}$, $\tilde{A}$ and $\tilde{B}$ states dissociate exclusively to CF_3^+, but the $\tilde{C}$ and $\tilde{D}$ states show coincidences for both CF_2^+ and CF_3^+ (Fig. 2). Third, now using the 5 m McPherson monochromator, we have studied fragmentation of the $\tilde{C}$ and $\tilde{D}$ states of CF_4^+ by the energy-scanning TPEPICO technique in some detail [17], since these

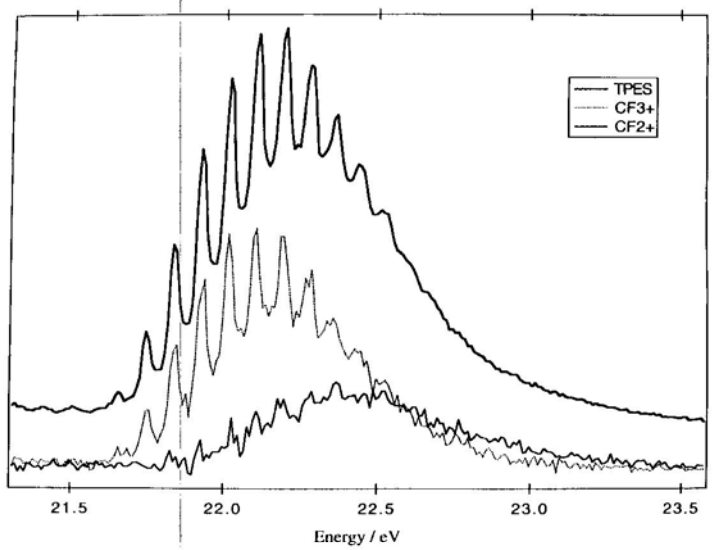

Fig. 6. Threshold photoelectron spectrum and coincidence yields of CF_3^+ and CF_2^+ from CF_4 excited into the $\tilde{C}\ ^2T_2$ ionic state between 21.4 and 23.5 eV. The photon resolution is 0.05 nm or ca. 0.02 eV. (Reproduced by permission from J. Chem. Phys. **101** (1994) 10559).

states exhibiting vibrational structure in their photoelectron spectra are most amenable to high-resolution study. Fig. 5 shows the three-dimensional false-colour TPEPICO spectrum of the $\tilde{C}\ ^2T_2$ state of CF_4^+ recorded in the energy-scanning mode at a photon resolution of ca. 0.02 eV. As noted above and in our previous work [28], CF_3^+ and CF_2^+ are the fragment ions observed, and their yields are displayed in Fig. 6 together with the threshold photoelectron signal.

From these figures we can make the following observations. First, the long vibrational progression in the photoelectron spectrum is the ν_1 symmetric C-F stretching vibration of a_1 symmetry. We determine an adiabatic IP for the CF_4^+ $\tilde{C}$ state of 21.656 ± 0.006 eV and an average vibrational spacing of 0.090 ± 0.005 eV or 726 ± 40 cm^{-1}. This latter value is in excellent accord with that determined from the higher-resolution optical study of the $\tilde{D}$-$\tilde{C}$ transition in CF_4^+ of 729 ± 1 cm^{-1} [31]. At the resolution of 0.02 eV we see no evidence for other vibrational bands contributing to the structure of the photoelectron band, and we conclude that any Jahn-Teller distortion of this orbitally-degenerate T_2 state from tetrahedral symmetry is minimal. Structure in the ν_1 vibration is lost for $\nu_1 > 10$, suggesting that higher vibrational levels dissociate or predissociate at a rate greater than ca. 10^{13} s^{-1}. Second, the yield of CF_3^+ exactly mirrors the threshold photoelec-

tron signal, with vibrational structure in ν_1 being observed for the first time in the ion yield. Since the yield has an identical shape and structure to the Franck-Condon envelope of the CF_4^+ $\tilde{C}$ state, we believe that the predominant route for production of this ion is an indirect, two-step process, i.e. radiative decay of the CF_4^+ $\tilde{C}$ state to the repulsive $\tilde{X}$ and $\tilde{A}$ states followed by direct dissociation to CF_3^+. Evidence to support this suggestion comes from two sources: the $\langle KE \rangle_t$ values from the $\tilde{X}$, $\tilde{A}$ and $\tilde{C}$ states of CF_4^+ dissociating to $CF_3^+ + F$ all show similar values (Table 2) despite the three electronic states being over 6 eV apart in energy, and a PIFCO spectrum at the CF_4^+ $\tilde{C}$ state shows a signal only at the mass-to-charge ratio of the CF_3^+ ion (see below). Third, the CF_2^+ ion, unlike CF_3^+, arises from a competing dissociative process of the CF_4^+ $\tilde{C}$ state. It seems very likely that this process is non-radiative, because the $\tilde{X}$, $\tilde{A}$ and $\tilde{B}$ states of CF_4^+ (to which $\tilde{C}$-state fluorescence might occur) all lie below the lowest thermochemical energy producing CF_2^+ (Fig. 3). The yield of CF_2^+ shows a gradual rise with a threshold at 21.85 ± 0.05 (a slightly higher energy than that of CF_3^+) corresponding to the energy of $\nu_1 = 2$, a maximum ca. 0.3 eV to higher energy than that of the CF_3^+ ion, and partially-resolved vibrational structure in the ν_1 band. We believe that the CF_2^+ signal may arise from a direct dissociation, probably involving the formation of a tightly-constrained transition state at a barrier along the dissociation coordinate. By analogy with calculations on the $\tilde{A}\ ^1T_2$ lowest Rydberg state of CH_4 [36], it is possible that the $\tilde{C}\ ^2T_2$ state of CF_4^+ correlates adiabatically to the ground state of CF_2^+ ($\tilde{X}\ ^2A_1$) and F_2 ($X\ ^1\Sigma_g^+$). Excited states of CF_2^+ cannot form on energetic grounds [37]. Assuming that the CF_3^+ signal arises solely from the radiative decay process described above, then at any photon energy the ratio of the CF_3^+ yield to that of CF_2^+ gives the ratio of $(\Phi_F)_v$ to $[1\text{-}(\Phi_F)_v]$. Thus we obtain $(\Phi_F)_v$ = 1, 1, 0.90, 0.91, 0.87, 0.82, 0.77, 0.72, 0.63, 0.61 and 0.53 for $v_1 = 0-10$, respectively. The integrated area of the CF_3^+ signal to the CF_2^+ signal yields a vibrationally-averaged value for the fluorescence quantum yield of the CF_4^+ $\tilde{C}$ state of $(\Phi_F)_{average} = 0.67 \pm 0.05$. Although not a direct comparison, this confirms the value of 0.5 ± 0.4 obtained from the fluorescence excitation spectrum at an energy of 22.6 eV (Section 5.1).

Fluorescence coincidence experiments allow us to obtain absolute values for $(k_{rad})_v$ and $(k_{non\text{-}rad})_v$ for individual ν_1 vibrational levels of the CF_4^+ $\tilde{C}$ state. A PIFCO spectrum recorded at the Franck-Condon maximum of the $\tilde{C}$ state with the Seya monochromator shows that coincidences are only observed with ions whose TOF corresponds to that of CF_3^+ [8]. Thus, as expected, fluorescence from the CF_4^+ $\tilde{C}$ state occurs to the lower-lying $\tilde{A}$ $^2T_2$ and $\tilde{X}\ ^2T_1$ states which dissociate directly to CF_3^+. More informative, however, is to measure vibrationally-state-selected lifetimes (τ_v) of the CF_4^+ $\tilde{C}$ state by the TPEFCO technique. Fig. 7 shows TPEFCO spectra recorded at four different photon energies within the CF_4^+ $\tilde{C}$ state, namely 21.84, 22.02, 22.20 and 22.36 eV corresponding to v_1 = 2, 4, 6 and 8,

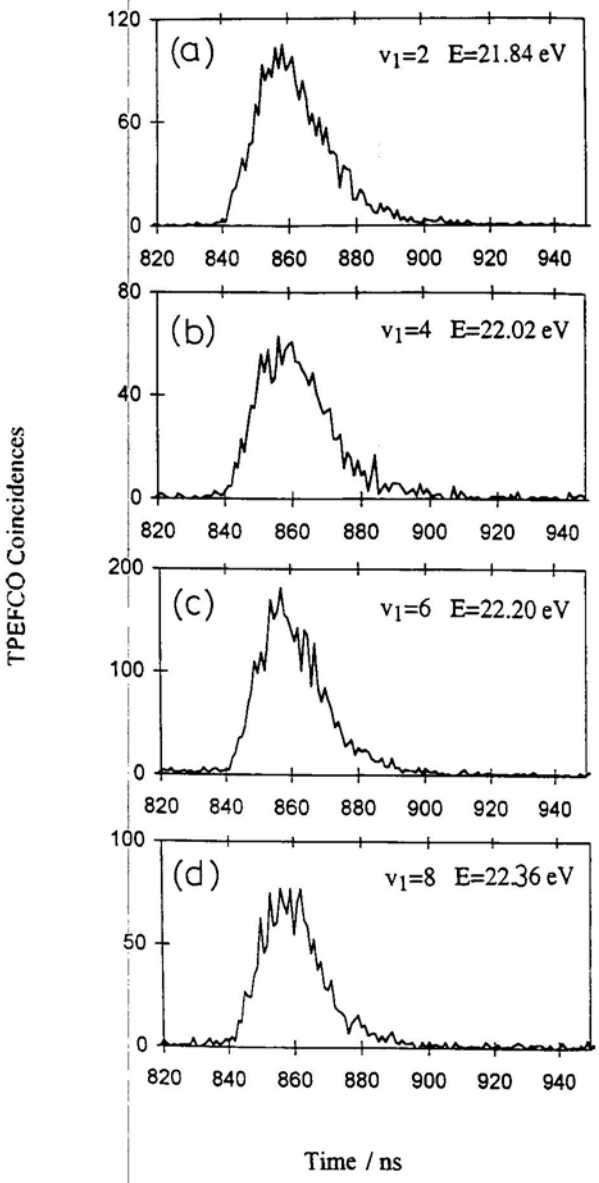

Fig. 7. TPEFCO spectra of the fluorescence from the $\tilde{C}\ ^2T_2$ state of CF_4^+ at excitation energies of (a) 21.84, (b) 22.02, (c) 22.20, and (d) 22.36 eV, corresponding to v_1 = 2, 4, 6, and 8, respectively. The photon resolution is 0.05 nm or ca. 0.02 eV, the time resolution is 1 ns per channel, and the accumulation time of each spectrum is ca. 5 h. The fluorescence 'stop' pulses are delayed by 860 ns to separate the almost simultaneous start and stop pulses at the TDC, explaining the offset in the time axis. (Reproduced by permission from J. Chem. Phys. **101** (1994) 10559).

Table 3. Fluorescence quantum yields $(\Phi_F)_v$, lifetimes τ_v, and radiative (k_{rad}) and non-radiative ($k_{non\text{-}rad}$) decay rates of vibrational levels of CF_4^+ $\tilde{C}$ $^2T_2$[a].

v_1	E/eV	CF_3^+/CF_2^+	$(\Phi_F)_v$[b]	τ_v/ns	$k_r(10^8\ s^{-1})$[c]	k_{nr} $(10^8\ s^{-1})$[d]
0	21.66	∞	1			
1	21.75	∞	1			
2	21.84	12.0 ± 2.0	0.92 ± 0.20	9.0 ± 0.3	1.0 ± 0.2	0.09 ± 0.02
3	21.93	10.4 ± 0.9	0.91 ± 0.08			
4	22.02	6.9 ± 0.4	0.87 ± 0.04	8.6 ± 0.4	1.01 ± 0.07	0.15 ± 0.01
5	22.11	4.5 ± 0.1	0.82 ± 0.02			
6	22.20	3.3 ± 0.1	0.77 ± 0.02	8.4 ± 0.3	0.92 ± 0.04	0.27 ± 0.01
7	22.28	2.57 ± 0.06	0.72 ± 0.01			
8	22.36	1.69 ± 0.03	0.63 ± 0.01	7.9 ± 0.4	0.80 ± 0.03	0.47 ± 0.02
9	22.41	1.54 ± 0.03	0.61 ± 0.01			
10	22.52	1.13 ± 0.03	0.53 ± 0.01			

[a] Taken from Ref. [17].
[b] Calculated assuming the ratio of the CF_3^+ to CF_2^+ signal is $(\Phi_F)_v/[1\text{-}(\Phi_F)_v]$.
[c] Calculated from $k_{rad} = (\Phi_F)_v/\tau_v$.
[d] Calculated from $k_{non\text{-}rad} = [1\text{-}(\Phi_F)_v]/\tau_v$.

respectively. No filter was used with the photomultiplier, and a 1 ns resolution of the time-to-digital converter was used. The lifetimes of these four levels decrease monotonically from 9.0 to 7.9 ns as v_1 increases from 2 to 8. Thus, as intimated by the time-resolved fluorescence experiments (Section 5.1), τ_v does change with vibrational quantum number, and the only real surprise is that the change in τ_v is so small. $(k_{rad})_v$ and $(k_{non\text{-}rad})_v$ are related to the observables $(\Phi_F)_v$ and τ_v by

$$(k_{rad})_v = (\Phi_F)_v/\tau_v \text{ and } (k_{non\text{-}rad})_v = [1\text{-}(\Phi_F)_v]/\tau_v \,. \quad (6)$$

The TPEPICO data (Fig. 6) show clearly that $(\Phi_F)_v$ decreases as photon energy within the CF_4^+ $\tilde{C}$ state (or v_1) increases. Hence for τ_v to vary so little with v_1, as v_1 increases k_{rad} must decrease at approximately the same rate as $k_{non\text{-}rad}$ increases to maintain $(k_{rad} + k_{non\text{-}rad})$ approximately constant. The absolute values for k_{rad} and $k_{non\text{-}rad}$ for the four values of v_1 are shown in Table 3. The small values of $k_{non\text{-}rad}$ must arise through slow intramolecular vibrational redistribution within the CF_4^+ $\tilde{C}$ state. Photoionisation only populates the v_1 (a_1) manifold, whereas dissociation to CF_2^+ must involve channeling the energy into the v_2 (e) vibrational mode. This process is relatively slow (ca. $10^7 - 10^8\ s^{-1}$), allowing fluorescence to be a significant, competing decay pathway. The non-radiative process is presumably hindered by the high symmetry of the $\tilde{C}$ state and the corresponding low density of vibrational levels, and there is no Jahn-Teller distortion of the $\tilde{C}$ $^2T_2$ state to lower symmetry to 'drive' this channel. Furthermore, the large gap of 2.5 eV between the $\tilde{C}$ and $\tilde{B}$ states also hinders internal conversion, so the $\tilde{C}$ state exhibits many of the properties of an isolated state. $k_{non\text{-}rad}$ increases

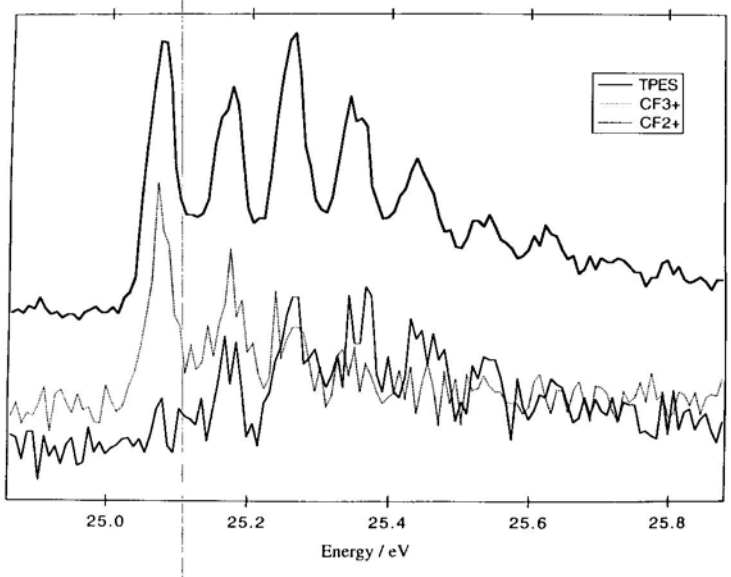

Fig. 8. Threshold photoelectron spectrum and coincidence yields of CF_3^+ and CF_2^+ from CF_4 excited into the $\tilde{D}\ ^2A_1$ ionic state between 24.9 and 25.8 eV. The photon resolution is 0.05 nm or ca. 0.026 eV. (Reproduced by permission from J. Chem. Phys. **101** (1994) 10559).

for higher values of ν_1 (Table 3) due to an increase in the density of vibrational levels as the barrier to dissociation is approached. This interpretation is substantiated by an analysis of Doppler-limited optical emission spectra of different vibronic bands of the $\tilde{D}$ ($\upsilon_1' = 0$) $-$ $\tilde{C}(\upsilon_1'')$ transition in CF_4^+ [38]. Perturbations become increasingly apparent in the rotational structure of the $\tilde{C}$ state as υ_1'' increases, becoming marked for $\upsilon_1'' \geqslant 2$ as non-radiative processes become more important.

Fig. 8 shows an energy-scanning TPEPICO spectrum of the $\tilde{D}\ ^2A_1$ state of CF_4^+ at a photon resolution of ca. 0.03 eV. Again CF_3^+ and CF_2^+ are the fragment ions observed. The TPES shows a long progression in ν_1 extending up to $\upsilon_1 = 5$ or 6, and values for ν_1 of 0.093 ± 0.007 eV or 750 ± 56 cm^{-1} and an adiabatic IP of 25.074 ± 0.008 eV are obtained. The TPES shows a very different vibrational intensity structure to the He II photoelectron band [29], where direct ionisation to $\upsilon_1 = 0$ is the strongest peak and only very weak bands to $\upsilon_1 > 0$ are observed. Clearly autoionisation via high-lying Rydberg states of CF_4 around 25 eV contributes by an indirect process to the TPE signal, resulting in an anomalous non-Franck-Condon vibrational distribution. Interpretation of the origin of the fragment ions is less clear than for the $\tilde{C}$ state. We assume that all the CF_3^+ yield again arises indirectly from radiative decay of the $\tilde{D}$ state to the repulsive $\tilde{A}$ state of CF_4^+ which

dissociates to CF_3^+, and that the CF_2^+ yield arises via internal conversion into high vibrational levels of the $\tilde{C}$ state prior to direct dissociation. If this is the case, then as before we can obtain $(\Phi_F)_v$ values of 0.9, 0.57, 0.36, 0.29, 0.18, 0.20 and 0.2 for $v_1 = 0-6$ respectively, and a vibrationally-averaged value for the fluorescence quantum yield of 0.38 ± 0.02. PIFCO and TPEFCO experiments on the CF_4^+ $\tilde{D}$ state were not performed for two reasons. First, the partial ionisation cross-section into this state is relatively small [34]. Second, the one previous measurement of its lifetime by a phase-shift technique (2.1 ns [32]) suggests that it is too short to be measured accurately in a fluorescence coincidence experiment with an optimum TDC resolution of 1 ns and a photomultiplier response time of 1.5 ns.

The observation of radiative decay from the $\tilde{C}$ and $\tilde{D}$ states of CF_4^+, and the fact that fragmentation of these states occurs to CF_2^+ (and not to the lower-energy CF_3^+ channel) are examples of non-statistical behaviour in these states. The $\tilde{X}$, $\tilde{A}$ and $\tilde{B}$ states of CF_4^+ which dissociate to $CF_3^+ + F$, however, also show non-statistical behaviour as deduced from their $\langle KE \rangle_t$ values. In Table 4 we compare the experimental fraction of the available energy channelled into translational energy of the products with that calculated by the two limiting models in Section 4. The calculations are critically dependent on the energy of the $CF_3^+ + F$ channel and hence the IP of the CF_3 radical. This is a difficult quantity to measure because CF_3 changes from pyramidal to planar geometry upon ionisation, and no high-quality photoelectron spectrum of this radical has yet been reported. The most recent experimental results from ion-molecule studies suggest a value of 8.6 eV [39] and a very recent *ab initio* calculation gives 8.98 eV [40], both values substantially lower than 9.25 eV which was the accepted value from photoionisation mass spectrometry [41] for over two decades prior to 1990. Assuming the lowest value of 8.6 eV is correct, then the energy of $CF_3^+ + F$ occurs at 14.2 eV (Fig. 3). Our value of $\langle KE \rangle_t = 0.97$ eV when CF_4 is excited at 16.3 eV into the $\tilde{X}\ ^2T_1$ ionic state means that 46% of the available energy is channelled into translation. Using the same vibrational frequencies for CF_3^+ as pertain to the isoelectronic molecule BF_3 [42], the statistical model of Klots [25] calculates that only 13% should be channelled into translation. The impulsive dissociation model assuming a late release of energy (i.e. dissociation occurs after the CF_3^+ ion has relaxed to planar geometry) calculates this percentage to be 49%. Note that if the energy release is early, the fragment ion still retains some of its C_{3v} symmetry and it can have up to 0.5 eV bound up in vibrational energy [43]; E_{avail} is then correspondingly reduced by ca. 0.5 eV, and the fraction observed in translational energy of products is somewhat higher than the values shown in column 6 of Table 4. Similar comparisons can be made for the $\tilde{A}\ ^2T_2$ and $\tilde{B}\ ^2E$ states of CF_4^+. The conclusion from these results is that the $\tilde{X}$ and $\tilde{A}$ states dissociate essentially in a direct, non-statistical manner from repulsive potential energy surfaces. Since the KE releases from the $\tilde{A}$ and $\tilde{B}$ states are so

Table 4. Comparison of mean energy releases for F or Cl loss from CF_4^+, CF_3Cl^+ and CF_3Br^+ with those predicted from a statistical and an impulse dissociation model.

Daughter ion/ neutral	Parent ion and state	$h\nu$/ eV	$\langle KE\rangle_t$/eV	E_{avail}/ eV[a]	Fraction$_{expt}$[b]	Fraction$_{stat}$[c]	Fraction$_{impulse}$[d]
CF_3^+	CF_4^+ $\tilde{X}$	16.3	0.97 (5)	2.1	0.46 (2)	0.13	0.49
CF_3^+	CF_4^+ $\tilde{A}$	17.5	1.19 (4)	3.3	0.36 (1)	0.13	0.49
CF_3^+	CF_4^+ $\tilde{B}$	18.6	1.27 (14)	4.4	0.29 (3)	0.13	0.49
CF_3^+	CF_3Cl^+ $\tilde{X}$	13.25	0.11 (1)	0.97	0.11 (1)	0.13	0.38
CF_3^+	CF_3Cl^+ $\tilde{A}$	15.20	0.88 (5)	2.92	0.30 (2)	0.13	0.38
CF_3^+	CF_3Cl^+ $\tilde{B}$	15.85	0.69 (11)	3.57	0.19 (4)	0.13	0.38
CF_3^+	CF_3Cl^+ $\tilde{C}$	16.55	0.68 (11)	4.27	0.16 (3)	0.13	0.38
CF_3^+	CF_3Cl^+ $\tilde{D}$	17.61	0.79 (10)	5.33	0.15 (2)	0.13	0.38
CF_2Cl^+	CF_3Cl^+ $\tilde{B}$	15.85	1.08 (23)	2.32	0.47 (9)	ca. 0.125	0.47
CF_2Cl^+	CF_3Cl^+ $\tilde{C}$	16.55	1.24 (13)	3.02	0.41 (4)	ca. 0.125	0.47
CF_2Cl^+	CF_3Cl^+ $\tilde{D}$	17.61	1.23 (12)	4.08	0.30 (3)	ca. 0.125	0.47
CF_3	CF_3Cl^+ $\tilde{F}$	21.28	0.91 (6)	4.60	0.20 (1)	0.13	0.38
CF_3^+	CF_3Br^+ $\tilde{X}$	12.23	0.05 (3)	0.65	0.08 (5)	0.13	0.28
CF_3^+	CF_3Br^+ $\tilde{A}$	14.23	0.53 (4)	2.65	0.20 (2)	0.13	0.28
CF_2Br^+	CF_3Br^+ $\tilde{B}/\tilde{C}$	16.33	1.10 (14)	2.32	0.47 (6)	ca. 0.125	0.44
CF_2Br^+	CF_3Br^+ $\tilde{D}$	17.53	0.99 (13)	3.52	0.28 (4)	ca. 0.125	0.44

[a] E_{avail} is the photon energy minus the dissociation energy of a particular fragmentation channel.

[b] Given by $\langle KE\rangle_t/E_{avail}$. It is assumed that all the error is in the experimental $\langle KE\rangle_t$, and none in E_{avail}, i.e. there is no error in the thermodynamic thresholds (see text).

[c] Calculated from the phase space, statistical theory due to Klots [25]. See Eq. (3) and Section 4 of text.

[d] Calculated from the impulse dissociation model of Riley and Wilson [24]. See Eq. (4) and Section 4 of text.

similar and these states lie only 1 eV apart, it seems likely that the $\tilde{B}$ state dissociates via internal conversion into the $\tilde{A}$ state. Note that in Table 4 we do not compare values for the $\tilde{C}$ $^2T_2$ and $\tilde{D}$ $^2A_1$ states because here the CF_3^+ product does not arise from a direct fragmentation, but by an indirect process via fluorescence to the $\tilde{X}$ and $\tilde{A}$ states. This explains why the KE releases to $CF_3^+ + F$ from the $\tilde{X}$, $\tilde{A}$, $\tilde{C}$ and $\tilde{D}$ states are surprisingly similar (Table 2) given that these states lie up to 9 eV apart. Whilst the data for the $\tilde{C}$ and $\tilde{D}$ states of CF_4^+ lying above the energy of the He I line is new, that for the $\tilde{X}$, $\tilde{A}$ and $\tilde{B}$ states is in excellent agreement with data from other groups [43–45].

5.3 TPEPICO experiments on the valence states of CF_3Cl^+ and CF_3Br^+

We have made an extensive study by fixed-energy TPEPICO spectroscopy of the KE releases from fragmentation of the outer-valence electronic states of CF_3Cl^+ and CF_3Br^+ [10], measuring $\langle KE \rangle_t$ at the Frank-Condon maximum of all such states (Table 4). The lower symmetry of these ions, C_{3v}, compared to tetrahedral ions such as CF_4^+ means that there are a larger number of valence states covering the same range of energy, hence it might be expected that radiative decay from excited states is a less important decay channel. This is indeed the case, and only the $\tilde{E}\ ^2A_1$ state of CF_3Cl^+ (which 'evolves' directly from the C $^2T_2$ state of a corresponding tetrahedral ion) shows radiative decay to any extent [46, 47]. We have not been able to measure the fluorescence quantum yield of this state, but it is probably only of the order 10^{-1} to 10^{-2}. Radiative decay therefore makes very little difference to the analysis and interpretation of the KERD results, a resume of which are presented here.

The electron configuration of the eight highest-occupied outer-valence molecular orbitals of CF_3X (X = Cl, Br) is $\ldots (3a_1)^2(2e)^4(4a_1)^2(3e)^4(4e)^4(1a_2)^2(5a_1)^2(5e)^4$, where the numbering scheme is restricted to those MOs formed from the valence atomic orbitals of C (2s,2p), F (2s,2p), Cl (3s,3p) and Br (4s,4p). He I and He II photoelectron spectra have been reported by Cvitas *et al.* [48, 49]. The three fluorine lone-pair AOs have symmetry $a_1 + a_2 + 2e$, whilst the chlorine or bromine lone pair has symmetry e. *Ab initio* calculations using various basis sets [50] have allowed a qualitative description of the character of the individual valence MOs. Thus the 5e orbital is essentially comprised of a lone pair on the X atom, and therefore the IP of this orbital changes between CF_3Cl (13.1 eV) and CF_3Br (12.1 eV). The $5a_1$ orbital is associated with C−X σ-bonding, so again its energy drops (by ca. 1 eV) between CF_3Cl and CF_3Br. The $1a_2$, 4e, 3e and $4a_1$ orbitals are all essentially F 2p lone-pair orbitals, so their energies are invariant between CF_3Cl and CF_3Br although the small participation in C−F bonding character of these orbitals increases with increasing ionisation energy. The 2e orbital is bonding on the CF_3 moiety, whereas the $3a_1$ orbital is both C−F and C−X σ-bonding in character [51]. The overall assignment is confirmed by the similarity, both in relative intensities and peak positions, of the third to eighth bands in the He II photoelectron spectra of CF_3Cl and CF_3Br. Partial vibrational structure is only resolved in the $\tilde{D}\ ^2E$ and $\tilde{E}\ ^2A_1$ states of CF_3X^+ [48, 49].

The thermochemistry of these two systems is subtly different from that in CF_4^+, in that now the lowest dissociation channel to $CF_3^+ + X$ (energy = 12.28 and 11.58 eV for X = Cl and Br, respectively) lies only slightly below the Franck-Condon-excited region of the CF_3X^+ ground state. Indeed there is clear evidence that in both ions some parts of the ground-state potential do lie below this dissociation limit. KE releases in the fragmenta-

tion of the $\tilde{X}\ ^2E$ state of the two ions are therefore small, and in so far as can be established they conform relatively closely to the statistical limit (Table 4). This confirms earlier work of Powis and Danby [52] who analysed the detailed form of the $P(\varepsilon_t)$ vs. ε_t KERD for photon energies within the ground-state potential and showed that dissociation to $CF_3^+ + X$ is essentially statistical. Note that at the photon energies at which our measurements were taken (13.25 eV for CF_3Cl^+, 12.23 eV for CF_3Br^+), dissociation to $CF_2X^+ + F$ (energy = 13.53 and 14.01 eV for X = Cl and Br, respectively) is a closed channel. It is in the dissociation of excited electronic states of CF_3X^+ that non-statistical effects are apparent, and the $\langle KE \rangle_t$ values suggest that there is a relationship between the part of the parent molecule where ionisation occurs and the bond that breaks to form the daughter ion + atom products. Some of these effects were observed fifteen years ago by Powis [43], and we have extended and improved his data.

On energetic grounds, dissociation of the $\tilde{A}\ ^2A_1$ first excited state of either ion can occur to both $CF_3^+ + X$ and $CF_2X^+ + F$, but the only channel observed is X-atom loss to CF_3^+. For CF_3Cl^+ $\tilde{A}$ the fraction of the available energy released into translational KE (0.30 ± 0.02) is much closer to the prediction of the impulsive model than the statistical model (Table 4), and if the dissociation is early, the fraction rises to ca. 0.36, very close to the impulsive prediction of 0.38. For CF_3Br^+ $\tilde{A}$ the result is not quite so clear in that the experimentally-observed fraction (0.20 ± 0.02) lies midway between the limiting statistical and impulsive models. Ionisation to the $\tilde{A}$ state involves removal of a σ-bonding C-X electron. Since this is the bond that breaks to give the $CF_3^+ + X$ products, it is perhaps not surprising that a statistical model does not fit the data at all well, and an impulsive dynamical model is more appropriate. Put another way, a consequence of such direct dynamics is that the $\tilde{A}$ state does not have time to couple efficiently with the ground state of the ion via internal conversion (the precursor to a statistical dissociation from the ground-state potential energy surface), hence the F-atom loss channel to CF_2X^+, despite being energetically open, is not observed.

The $\tilde{B}$ state of neither CF_3Cl^+ nor CF_3Br^+ is well resolved in the threshold photoelectron spectrum [10]. In the former case it sits on the high-energy shoulder of the $\tilde{A}$-state band, in the latter on the low-energy shoulder of the $\tilde{C}$ state band. It is therefore difficult to perform a true-state-selected study on the fragmentation dynamics of this state. The $\tilde{B}$, $\tilde{C}$ and $\tilde{D}$ states of CF_3X^+ arise essentially from removal of a F lone-pair electron. At the energies of the $\tilde{C}$ and $\tilde{D}$ states, dissociation to both CF_3^+ and CF_2X^+ is observed, although in his earlier study Powis [43] was only able to observe the stronger CF_2X^+ channel. This is surprising because at 16.55 and 17.61 eV, the Franck-Condon maxima of the $\tilde{C}$ and $\tilde{D}$ states of CF_3Cl^+, we measure the CF_3^+ yield to be ca. 30 and 40% respectively of the CF_2Cl^+ yield (Fig. 9). For the $\tilde{B}$ and $\tilde{C}$ states of CF_3X^+, Table 4 shows that if the C-X

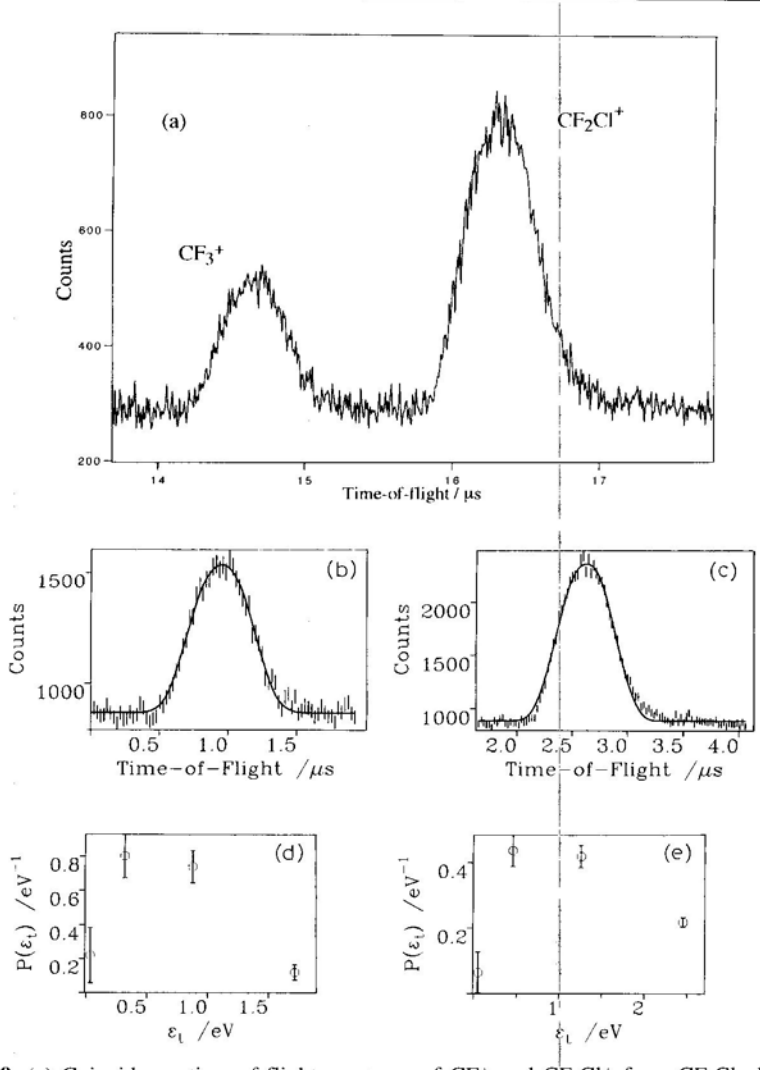

Fig. 9. (a) Coincidence time-of-flight spectrum of CF_3^+ and CF_2Cl^+ from CF_3Cl photoionised at 17.61 eV into the $\tilde{D}$ ^2E state of the parent ion. The time resolution is 8 ns per channel, and the accumulation time is 8 h. (b) and (c) Simulations of the CF_3^+ and CF_2Cl^+ peaks using the method of Powis *et al.* [20]. To improve the statistics of the fit, three successive datapoints are added. Zero time-of-flight corresponds to 13.7 μs in (a). (d) and (e) The probability distribution functions obtained from (b) and (c) (see text), yielding $\langle KE \rangle_t$ values of 0.79 ± 0.10 and 1.23 ± 0.12 eV, respectively. (Reproduced by permission from J. Phys. Chem. **100** (1996) 4350).

bond breaks to form CF_3^+ + X, the fraction of energy released into translation is much closer to the statistical limit than to the impulse dynamical limit. Conversely, if a C−F bond breaks to form CF_2X^+ + F then the frac-

tion of the available energy released into translation is greater and is much closer to the impulsive limit of 0.47. Given that the electron is removed from a F lone-pair orbital adjacent to a C−F bond, intuitively it seems sensible that the lifetime of the $\tilde{B}$ and $\tilde{C}$ electronic states of CF_3X^+ will be greater if dissociation occurs through cleavage of the C−X bond than through cleavage of a C−F bond. Hence it is not surprising that dissociation to CF_3^+ shows a more statistical translational energy release than dissociation to CF_2X^+. However, for the $\tilde{D}$ state of both parent ions, whilst dissociation to $CF_3^+ + X$ is still essentially statistical, the fraction of translational KE released into $CF_2X^+ + F$ lies midway between the statistical and the impulsive limits (Table 4). This result is compatible with the increased CF_3 bonding character of the 3e molecular orbital compared to the 4e and $1a_2$ orbitals, because in the former case the charge is distributed over the whole of the CF_3 moiety rather than being localised on a F lone-pair atomic orbital. Finally from Table 4, we note that the fraction of energy released into translational energy of a minor channel, $Cl^+ + CF_3$, from dissociation of the $\tilde{F}\ ^2E$ state of CF_3Cl^+ lies closer to the statistical than the impulsive limit. Given that the 2e orbital is bonding on the CF_3 moiety, fragmentation through cleavage of the C−Cl bond can only occur following a significant redistribution of energy within the molecule, conditions under which a statistical KE release into products is likely.

Powis [43] has commented that in other aspects F-atom loss and dissociation of the $\tilde{B}$, $\tilde{C}$ and $\tilde{D}$ excited states of CF_3X^+ to $CF_2X^+ + F$ is essentially a non-statistical process. First, as we observe, dissociation is primarily to CF_2X^+ and *not* to the lower-energy CF_3^+ channel. This is an excellent example of the behaviour of an isolated state, and contradicts statistical theories which assume that internal conversion to the ground electronic state of the parent ion occurs very rapidly and prior to a much-slower dissociation process. Second, within a given electronic state Powis [43] found that $\langle KE \rangle_t$ is independent of vibrational excitation. This implies that the vibrational modes excited upon ionisation are not strongly coupled to the reaction coordinate (i.e. intramolecular vibrational redistribution is slow), so that energy randomisation cannot occur within the lifetime of the parent ion. Third, the shapes of the $P(\varepsilon_t)$ vs. ε_t KERDs obtained by Powis and by us are suggestive of a fast and direct rather than a slow and statistical dissociation. It would seem that, like CF_4^+, CF_3Cl^+ and CF_3Br^+ have not approached the large-molecule limit. If this were so, rapid internal conversion between the excited states would always lead to a statistical dissociation pattern occurring from the ground-state potential energy surface [3]. Since this is not the case, state-specific behaviour is both expected and observed, the most striking example in this section being the dissociation of the $\tilde{B}$, $\tilde{C}$ and $\tilde{D}$ states of CF_3X^+ mainly forming $CF_2X^+ + F$, and not $CF_3^+ + X$.

5.4 Fluorescence coincidence experiments involving excited states of $SiCl_4^+$ and BCl_3^+

The $SiCl_4^+$ cation is an excellent example of how a PIFCO spectrum can give information on the fate of the electronic state of the ion to which fluorescence occurs. The $\tilde{C}\ ^2T_2$ state of this ion (adiabatic IP = 15.1 eV) decays radiatively, a non-statistical process since fragmentation to both $SiCl_3^+$ and $SiCl_2^+$ is energetically possible. Both PIFCO and TPEFCO spectra have been recorded at the energy of the Franck-Condon maximum of this state [17]. The TPEFCO spectrum shows a single-exponential decay with a lifetime of 38 ns, in exact agreement with the value obtained by time-resolved fluorescence at various excitation energies within the $SiCl_4^+$ $\tilde{C}$ Franck-Condon region [4]. The invariance of τ with energy strongly suggests that Φ_F also is independent of energy, and the similar value of τ obtained by the cation-specific TPEFCO technique is good evidence both that $\tilde{C}$-state ionisation is the only process occuring at this photon energy, and that Φ_F is probably close or equal to unity. It is from the PIFCO spectrum, however, that most new information is revealed. As with CF_4^+, $\tilde{C}$-state fluorescence occurs both to the ground and the first excited state of the ion. However, unlike CF_4^+ where both $\tilde{X}$ and $\tilde{A}$ states are repulsive in the Franck-Condon region, the $\tilde{X}$ state of $SiCl_4^+$ is bound whereas the $\tilde{A}$ state is repulsive. This arises essentially because the $SiCl_3^+ + Cl$ dissociation energy (at 12.7 eV) lies midway between the $\tilde{X}$ and $\tilde{A}$ states of the parent ion. Fig. 10 shows three PIFCO spectra each recorded with different optical filtering in front of the red-sensitive photomultiplier tube. In Fig. 10(a) no filter is used, in Fig. 10(b) a Schott UG5 filter transmitting the range ca. 220−400 nm is used, and in Fig. 10(c) a Schott OG515 filter transmitting wavelengths greater than 500 nm is used. In Fig. 10(a) coincidences are observed with two ions whose mass-to-charge ratio corresponds to $SiCl_3^+$ and $SiCl_4^+$, in Fig. 10(b) only coincidences with $SiCl_4^+$ are observed, and in Fig. 10(c) only coincidences with $SiCl_3^+$ are observed. These measurements confirm that the final states of the two radiative processes originating from the $\tilde{C}$ state of $SiCl_4^+$ differ significantly; one results in a stable state of the parent ion ($\tilde{X}$) while the other produces the unstable $\tilde{A}$ state which fragments to $SiCl_3^+ + Cl$. In an earlier optical study with a resolution of 0.2 nm using electron-impact ionisation of a supersonic beam of $SiCl_4$ [53], two broad bands were observed with peaks at 410 and 570 nm. They were assigned to $SiCl_4^+$ $\tilde{C}$-$\tilde{X}$ and $\tilde{C}$-$\tilde{A}$, respectively, and both bands appeared to be continuous. This PIFCO study shows that the radiative process involving the UV emission must be interpreted as a bound-bound transition which has the appearance of a bound-free transition due to rovibronic spectral congestion. Indeed, a more detailed study of the two bands at close to Doppler-limited resolution shows a clear difference between them; the visible band is continuous, while the UV band has a large amount of discrete structure

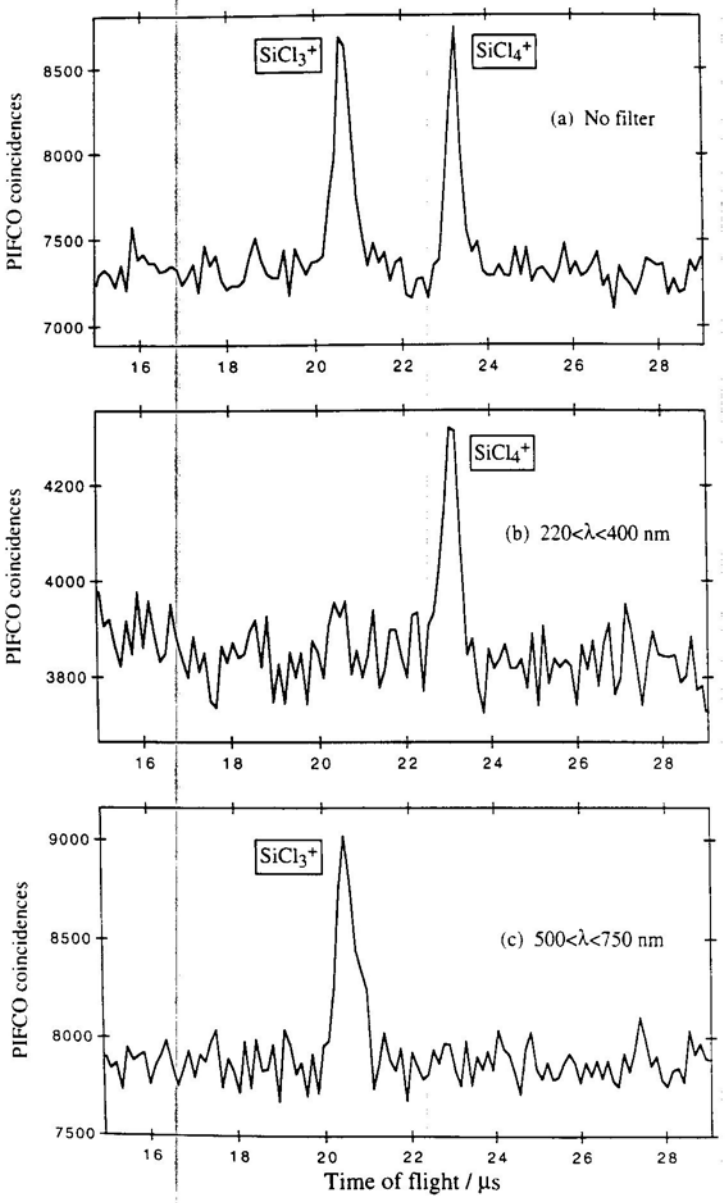

Fig. 10. PIFCO time-of-flight spectra of the fluorescence from the $\tilde{C}\ ^2T_2$ state of $SiCl_4^+$ at an excitation energy of 15.36 eV. The time resolution is 64 ns per channel and the accumulation time is ca. 8 h for each spectrum. In (a) no optical filter, in (b) a Schott UG5 filter transmitting the range 220−400 nm, and in (c) a Schott OG515 filter transmitting wavelengths greater than 500 nm is used with the Mullard 2254 QB photomultiplier tube. (Reproduced by permission from J. Chem. Phys. **101** (1994) 10559).

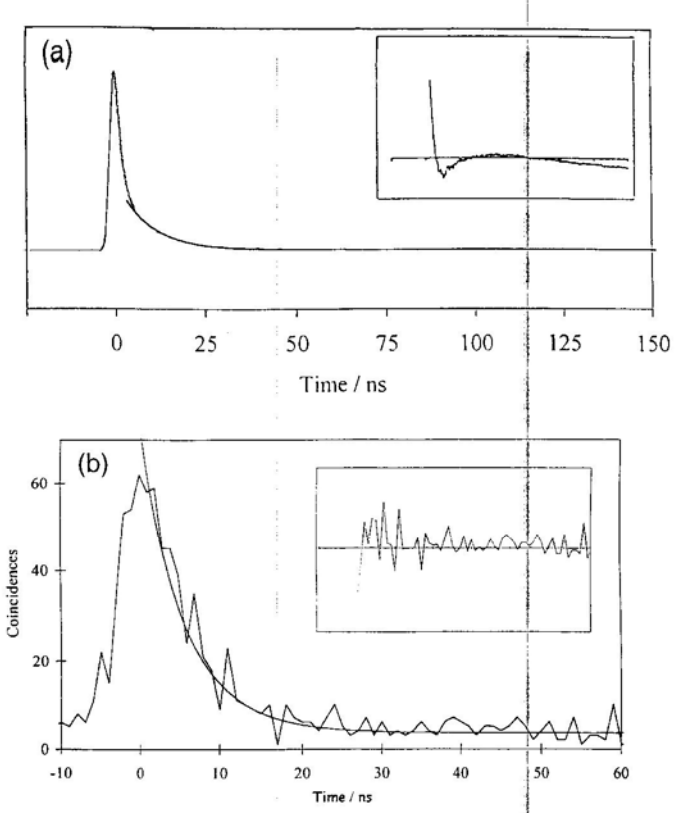

Fig. 11. (a) Decay of the fluorescence following excitation of BCl_3 at 15.58 eV. A Mullard 2020 QB tube (sensitivity range 200−500 nm) is used unfiltered. The solid line is the experimental data, the bold line a fit to the data using a single exponential, Poisson-weighted non-linear fitting procedure. A value of $\tau = 10.1 \pm 0.3$ ns is obtained [5]. The insert shows the residuals on the same time scale; note their *systematic* oscillations. (b) Threshold photoelectron-fluorescence coincidence spectrum of the fluorescence from the $\tilde{D}\ ^2E'$ state of BCl_3^+ at 15.51 eV. The time resolution is 1 ns per channel, the accumulation time is ca. 42 h, and no optical filter is used. A single exponential is drawn through the data with a rate constant of $1.8 \times 10^8\ s^{-1}$, corresponding to a lifetime of 5.5 ns [27]. The insert shows the *non-systematic* residuals on the same timescale as the decay. (Reproduced by permission from J. C. S. Faraday Trans. **91** (1995) 3073 and **92** (1996) 185).

[54]. The approximate equal intensities of the two ions in Fig. 10(a) must arise due to a near cancellation of two effects; the greater electronic transition moment of the $\tilde{C}$-$\tilde{A}$ transition (compared to $\tilde{C}$-$\tilde{X}$) is offset by the reduced quantum efficiency of the photomultiplier tube in the red region of the visible (where $\tilde{C}$-$\tilde{A}$ emission occurs) compared to that in the UV/blue visible (where $\tilde{C}$-$\tilde{X}$ emission occurs).

Finally, we discuss an interesting aspect of the TPEFCO coincidence spectra. Fluorescence from the $\tilde{D}\ ^2E'$ state of BCl_3^+ has been observed by fluorescence excitation [55], by dispersed emission [5] and by TPEFCO [27] spectroscopies. The lifetime of this state as revealed by the first-order decay of the TPEFCO spectrum is substantially different from that obtained by single-bunch fluorescence measurements of the kind reported for the $\tilde{C}$ state of CF_4^+ in Section 5.1. The non-state-specific time-resolved experiments gave non-single-exponential decays of the fluorescence for BCl_3 excited at 15.58 eV (the Franck-Condon maximum of the $\tilde{D}\ ^2E'$ state), and an 'average' value for the lifetime of 10.1 ± 0.3 ns was obtained [5] [Fig. 11(a)]. Dispersion of the emission induced at this photon energy is particularly revealing because, in addition to $\tilde{D}$-state emission from BCl_3^+, strong BCl A-X emission around 272 nm is also observed [5]. Thus, both non-resonant $\tilde{D}$-state ionisation and resonant excitation of Rydberg states of BCl_3 which photodissociate to the A $^1\Pi$ state of BCl are occurring at this photon energy. A time-resolved decay of the fluorescence will not, therefore, fit well to a single-exponential function because two emitters are present. Since the lifetime of the A state of BCl has been measured independently by the phase-shift method to be 19.1 ns [56], our 'average' value of 10.1 ns suggests that the lifetime of the BCl_3^+ $\tilde{D}$ state is less than this latter value. This is confirmed by the TPEFCO spectrum [Fig. 11(b)] where the lifetime of the $\tilde{D}$ state of the parent ion is measured to be 5.5 ± 0.5 ns. Note that in this technique the emission in the underlying *neutral* molecule (BCl) will only contribute to the background signal, and it is only emission in the *positively-charged* species that contributes to the signal. We also note that radiative decay of the BCl_3^+ $\tilde{D}$ state is a relatively minor channel, and an upper limit of the quantum yield, Φ_F, of 0.04 has been estimated [27]. This example shows the cation-specific TPEFCO spectrum can be used to deconvolute an ionic fluorescence lifetime from that of underlying neutral emissions. Note that with a VUV photoexcitation source of the correct energy, there are no contributions from cascading to the observed time-resolved decay, a phenomenon that is often observed using non-resonant electrons with much higher energy as the excitation source.

Table 5 shows the lifetimes we have measured to date for fluorescing states of molecular ions by the TPEFCO technique. For the N_2^+ B, CF_4^+ $\tilde{C}$, SiF_4^+ $\tilde{D}$ and $SiCl_4^+$ $\tilde{C}$ states, the values of τ obtained are very similar to those obtained by time-resolved fluorescence experiments using the single-bunch mode of the synchrotron. This strongly suggests that parent-ion formation is the dominant process occurring at the particular photon energy. However, for the BCl_3^+ $\tilde{D}$, CF_3H^+ and CF_3Cl^+ $\tilde{E}$ states, the lifetimes measured by the TPEFCO experiment are noticeably less than those measured by the single-bunch experiments, indicating that other (neutral) emission processes are contributing to the decays in the latter spectra.

Table 5. Comparison of the fluorescence lifetimes of emitting states of molecular ions measured by the TPEFCO technique and by time-resolved fluorescence experiments using the single-bunch mode of the synchroton.

Parent ion and state	$h\nu$/eV	τ(TPEFCO)/ns	τ(single-bunch)/ns	Reference
N_2^+ B $^2\Sigma_u^-$	18.8	61 ± 1	61 ± 1	
CF_4^+ $\tilde{C}$ $^2T_2$	21.8–22.4	9.0–7.9[a]		17
	21.9–25.6		9.7 – 8.6[b]	4
SiF_4^+ $\tilde{D}$ $^2A_1$	21.5–21.7	9 ± 2		17
	21.5–31.5		9.30 ± 0.04	4
$SiCl_4^+$ $\tilde{C}$ $^2T_2$	15.4	38 ± 1		17
	15.1–26.0		38.4 ± 0.1	4
BCl_3^+ $\tilde{D}$ $^2E'$	15.51	5.5 ± 0.5		27
	15.58		10.1 ± 0.3[c]	5
CF_3H^+ $\tilde{E}$ $^2A_1$	20.8	12.6 ± 0.8		47
	21.4		82 ± 4	58
CF_3Cl^+ $\tilde{E}$ $^2A_1$	20.2	9.4 ± 1.8		47
	21.0		26 ± 3	46
CF_3Br^+ $\tilde{E}$ $^2A_1$	20.0	no signal		47
	20.7		45 ± 1 and 17 ± 1[d]	59, 60

[a] Errors given in Table 3.
[b] Errors given in Table 1.
[c] 'Average' value. See text.
[d] Bi-exponential decay. Emission due to CF B ^2A, A $^2\Sigma^+$ and possibly other emitters.

6. Conclusions

In this paper we have described experiments to measure dynamic properties of state-selected vibronic states of medium-sized molecular ions whose size is intermediate between the small- and large-molecule limits. The main conclusions are as follows:

(a) The observation of radiative decay from high-lying valence electronic states of polyatomic ions is not confined to the highly-symmetrical tetrahedral species like CF_4^+. Fluorescence has now been observed from excited states of D_{3h} (e.g. BCl_3^+ and BBr_3^+ [55, 57]) and C_{3v} (e.g. CF_3H^+ and CF_3Cl^+ [58, 46]) symmetry, and preliminary experiments have observed such effects in some of the group V halides which also have C_{3v} symmetry (e.g. PCl_3^+). In all cases, emission is from states which lie at a higher energy than one or more ionic dissociation channel, and such 'isolated' states manifest non-statistical effects by their reluctance to couple efficiently via non-radiative processes with lower-lying electronic states of the parent ion, allowing radiative decay to be a competing pathway.

(b) The measurement of the lifetime of such an emitting state is best made by the TPEFCO technique which is specific to charged species. Errors can arise using the simpler time-resolved fluorescence technique with single-bunch mode of the synchrotron if parent-ion formation is not the dominant process at the appropriate photon energy. Like all absolute quantum yield measurements, values for the fluorescence quantum yield, Φ_F, of such states are difficult to determine, since such measurements need the calibration of the apparatus (be it fluorescence excitation or fluorescence coincidence) with a known ionic emitter.

(c) The combination of a continuously tunable photon source and the TPEPICO technique is a powerful tool for investigating fragmentation of electronic states of polyatomic ions. Perhaps most important, we can investigate all states with energies between 10 and 30 eV at a resolution that is governed essentially by that of the photon source; only with calibration studies on $(3p)^{-1}$ photoionisation of argon at 15.76 eV have we been able to approach the 4 meV resolution of the threshold electron analyser [17]. We are not limited to vibronic states of the parent ion below the energy of He I radiation (21.2 eV), and therefore are able to make a comprehensive study of fragmentation of the $\tilde{C}\ ^2T_2$ and $\tilde{D}\ ^2A_1$ states of CF_4^+; such measurements could only be made in a home laboratory using much-weaker He II radiation from a line source. This range of states that can be studied helps to counter the difficulties of working within limited time schedules at a synchrotron source. By measuring at a fixed photon energy the mean KE released into translational energy of the products, we are able to determine whether the fragmentation is essentially statistical or impulsive in character. A more detailed analysis of the KE release distribution is not possible due to the 300 K temperature of molecules along the axis of the TPEPICO apparatus. One improvement to the apparatus in the near future will be to reduce this effect as much as possible.

(d) What emerges most clearly from the fragmentation work is that when the ionic ground state is repulsive in the Franck-Condon region (CF_4^+ and SF_6^+ being the two best examples [28]), fragment ions have appearance energies at the adiabatic energies of electronic states of the parent ion, and not at the lowest thermodynamic threshold forming that ion. As commented earlier, this is not the expected pattern for a large polyatomic ion, but rather that which is observed for diatomic ions. For polyatomics the conventional view is that the initial photo-induced ionisation event serves only to create the molecular ion in a range of electronic states, with equilibration taking place so rapidly between the states that one need only consider the density of vibrational levels of the electronic ground state of the ion in determining the fragmentation pattern. In such statistical dissociations the fragment ions usually have thresholds very close to their thermodynamic energy, and any excess energy appears mainly as internal energy of the fragments, not as translational energy. However, since the ground

states of CF_4^+, SF_6^+, and many of the other ions we have studied are repulsive or, at best, possess only a very shallow minimum in the potential energy surface in the Franck-Condon region, such theories (e.g. QET) may not apply. These are circumstances, therefore, under which isolated-state behaviour and non-statistical effects may be observed in excited electronic states of the parent ion.

Acknowledgements

We thank the staff at the Daresbury Laboratory for considerable assistance, Dr. I. Powis (Nottingham University) for many helpful discussions and the extensive use of his kinetic energy analysis program, and Dr. M. Stankiewicz and Mr. K. R. Yoxall for help with many of the experiments. The UK Engineering and Physical Sciences Research Council is thanked for an equipment grant, an Advanced Fellowship (PAH), and a Post-Doctoral Fellowship (DMS). The European Union Human Capitol and Mobility Program (contract number CHGE-CT93-0027) and the British Council (ARC bilateral programme between Birmingham University and Professor Baumgärtel's group in Berlin) are also thanked for funding the dispersed fluorescence work at the BESSY synchrotron source.

References

1. J. P. Maier, Chimica **34** (1990) 219.
2. G. Herzberg, Quart. Rev. Chem. Soc. **25** (1971) 201.
3. H. M. Rosenstock, Adv. Mass Spectrom. **4** (1968) 523.
4. I. R. Lambert, S. M. Mason, R. P. Tuckett and A. Hopkirk, J. Chem. Phys. **89** (1988) 2683.
5. H. Biehl, J. C. Creasey, D. M. Smith, R. P. Tuckett, K. R. Yoxall, H. Baumgärtel, H. W. Jochims and U. Rokland, J. C. S. Faraday Trans. **91** (1995) 3073.
6. R. P. Tuckett, Chem. Soc. Rev. **19** (1990) 439.
7. P. A. Hatherly, M. Stankiewicz, K. Codling, J. C. Creasey, H. M. Jones and R. P. Tuckett, Meas. Sci. Tech. **3** (1992) 891.
8. P. A. Hatherly, K. Codling, D. M. Smith, R. P. Tuckett, K. R. Yoxall and J. F. M. Aarts, Chem. Phys. **174** (1993) 453.
9. J. C. Creasey, I. R. Lambert, R. P. Tuckett, K. Codling, L. J. Frasinski, P. A. Hatherly, M. Stankiewicz and D. M. P. Holland, J. Chem. Phys. **93** (1990) 3295.
10. J. C. Creasey, D. M. Smith, R. P. Tuckett, K. R. Yoxall, K. Codling and P. A. Hatherly, J. Phys. Chem. **100** (1996) 4350.
11. J. C. Creasey, Ph. D. Thesis, University of Birmingham (1992).
12. J. C. Creasey, I. R. Lambert, R. P. Tuckett, K. Codling, L. J. Frasinski, P. A. Hatherly and M. Stankiewicz, J. C. S. Faraday Trans. **87** (1991) 1287.
13. S. D. Price and J. H. D. Eland, J. Phys. B. **22** (1989) L153.
14. T. Baer, W. B. Peatman and E. W. Schlag, Chem. Phys. Lett. **4** (1969) 243.
15. R. I. Hall, A. McConkey, K. Ellis, G. Dawber, L. Avaldi and G. C. King, Meas. Sci. Tech. **3** (1992) 316.
16. M. Richard-Viard, O. Dutuit, M. Lavolee, T. Govers, P. M. Guyon and J. Durup, J. Chem. Phys. **82** (1985) 4054.

17. D. M. Smith, R. P. Tuckett, K. R. Yoxall, K. Codling, P. A. Hatherly, J. F. M. Aarts and M. Stankiewicz, J. Chem. Phys. **101** (1994) 10559.
18. W. C. Wiley and I. H. MacLaren, Rev. Sci. Instrum. **26** (1955) 1150.
19. P. Baltzer, Phys. Rev. A **45** (1992) 4374.
20. I. Powis, P. I. Mansell and C. J. Danby, Int. J. Mass Spec. Ion Phys. **32** (1979) 15.
21. J. Berkowitz, *Photoabsorption, photoionisation and photoelectron spectroscopy*, Academic Press, NY (1979).
22. J. L. Franklin, P. M. Hierl and D. A. Whan, J. Chem. Phys. **47** (1967) 3148; R. Stockbauer, Int. J. Mass Spec. Ion Proc. **25** (1977) 89.
23. T. Baer, Adv. Chem. Phys. **LXIV** (1986) 111.
24. S. J. Riley and K. R. Wilson, J. C. S. Faraday Disc. **53** (1972) 132.
25. C. E. Klots, J. Chem. Phys. **58** (1973) 5364.
26. D. M. Smith, R. P. Tuckett, K. R. Yoxall, K. Codling and P. A. Hatherly, Chem. Phys. Lett. **216** (1993) 493.
27. H. Biehl, K. J. Boyle, D. M. Smith, R. P. Tuckett, K. R. Yoxall, K. Codling, P. A. Hatherly and M. Stankiewicz, J. C. S. Faraday Trans. **92** (1996) 185.
28. J. C. Creasey, H. M. Jones, D. M. Smith, R. P. Tuckett, P. A. Hatherly, K. Codling and I. Powis, Chem. Phys. **174** (1993) 441.
29. C. R. Brundle, M. B. Robin and H. Basch, J. Chem. Phys. **53** (1970) 2196.
30. A. J. Yencha, A. Hopkirk, A. Hiraya, G. Dujardin, L. Hellner, M. J. Besnard-Ramage, R. J. Donovan, J. G. Goode, R. R. J. Maier, G. C. King and S. Spyrou, J. Electron. Spectrosc. Relat. Phenom. **70** (1994) 29.
31. S. M. Mason and R. P. Tuckett, Mol. Phys. **60** (1987) 761.
32. J. E. Hesser and K. Dressler, J. Chem. Phys. **47** (1967) 3443.
33. S. M. Mason and R. P. Tuckett, Mol. Phys. **62** (1987) 979.
34. T. A. Carlson, A. Fahlman, W. A. Svensson, M. O. Krause, T. A. Whitley, F. A. Grimm, M. N. Piancastelli and J. W. Taylor, J. Chem. Phys. **81** (1984) 3828.
35. E. Castellucci, G. Dujardin, S. Leach and R. P. Tuckett, Chem. Phys. Lett. **116** (1985) 125.
36. M. S. Gordon and J. W. Caldwell, J. Chem. Phys. **70** (1979) 5503; H. U. Lee and R. Janoschek, Chem. Phys. **39** (1979) 271.
37. J. M. Dyke, L. Golab, N. Jonathan, A. Morris and M. Okuda, J. C. S. Faraday Trans. 2. **70** (1974) 1828.
38. J. F. M. Aarts and J. H. Callomon, Mol. Phys. **81** (1994) 1383.
39. E. R. Fisher and P. B. Armentrout, Int. J. Mass Spectrom. Ion Proc. **101** (1990) R1.
40. M. Horn, M. Oswald, R. Oswald and P. Botschwina, Ber. Bunsenges. Phys. Chem. **99** (1995) 323.
41. C. Lifshitz and W. A. Chupka, J. Chem. Phys. **47** (1967) 3439.
42. G. Herzberg, *Electronic structure of polyatomic molecules*, Van Nostrand Co., NY (1966).
43. I. Powis, Mol. Phys. **39** (1980) 311.
44. I. G. Simm, C. J. Danby, J. H. D. Eland and P. I. Mansell, J. C. S. Faraday Trans. 2. **72** (1976) 426.
45. B. Brehm, R. Frey, A. Kustler and J. H. D. Eland, Int. J. Mass Spectrom. Ion Phys. **13** (1974) 251.
46. J. C. Creasey, I. R. Lambert, R. P. Tuckett and A. Hopkirk, Mol. Phys. **71** (1990) 1367.
47. H. Biehl, K. J. Boyle, D. M. Smith and R. P. Tuckett, Chem. Phys. (1996) submitted.
48. T. Cvitas, H. Gusten, L. Klasinc, J. Chem. Phys. **67** (1977) 2687.
49. T. Cvitas, H. Gusten, L. Klasinc, I. Novak and H. Vancik, Z. Naturforsch. **33a** (1978) 1528.
50. H. E. Popkie and J. J. Kaufman, Int. J. Quantum Chem. Symp. **11** (1977) 433.
51. J. D. Bozek, G. M. Bancroft, J. N. Cutler, K. H. Tan, B. W. Yates and J. S. Tse, Chem. Phys. **132** (1989) 257.

52. I. Powis and C. J. Danby, Chem. Phys. Lett. **65** (1979) 390.
53. I. R. Lambert, S. M. Mason, R. P. Tuckett and A. Hopkirk, J. Chem. Phys. **89** (1988) 2675.
54. J. F. M. Aarts, unpublished data.
55. J. C. Creasey, P. A. Hatherly, I. R. Lambert and R. P. Tuckett, Mol. Phys. **79** (1993) 413.
56. J. E. Hesser, J. Chem. Phys. **48** (1968) 2518.
57. H. Biehl, D. M. Smith, R. P. Tuckett, K. R. Yoxall, H. Baumgärtel, H. W. Jochims and U. Rokland, Mol. Phys. **87** (1996) 1199.
58. J. C. Creasey, I. R. Lambert, R. P. Tuckett and A. Hopkirk, Mol. Phys. **71** (1990) 1355.
59. J. C. Creasey, P. A. Hatherly, I. R. Lambert and R. P. Tuckett, Chem. Phys. Lett. **188** (1992) 223.
60. H. Biehl, K. J. Boyle, R. P. Tuckett, H. Baumgärtel and H. W. Jochims, Chem. Phys. (1996) submitted.